Chapter 1

Introduction

With the recent advances in high power lasers, the interaction of plasma with high intensity laser fields has become possible. A rapid progress in ultra high intensity lasers over last few decades has occurred due to the invention of chirped pulse amplification (CPA) [1, 2] where a laser pulse is first stretched in time before amplification and then recompressed to generate femtosecond duration laser pulses. Interaction of these short laser pulses with plasmas has made it possible to generate electrons with relativistic energies, thus opening up new areas of relativistic nonlinear optics and plasma physics. Propagation of an intense laser pulse through plasma make electrons quiver with relativistic velocities and the electron motion becomes nonlinear [3, 4]. This nonlinear interaction of intense laser pulses with plasmas gives rise to a wide range of phenomena such as laser plasma based accelerators [5, 6], X-ray laser [7, 8], inertial confinement fusion [9–11], harmonic radiation generation [12–14] and relativistic soliton formation [15–17].

1.1 Propagation of electromagnetic waves in plasmas

Let us consider an electromagnetic wave linearly polarized along $\hat{y}$ and propagating along z direction of the form

$$\vec{E} = \hat{y}E_0 exp(ikz - \omega t) \tag{1.1}$$

through a plasma of ambient electron density n_0 where E_0 is the peak electric field amplitude, k and ω are the wavenumber and frequency of the electromagnetic wave respectively. The ions are considered to be immobile due to their higher mass and hence they form a neutralizing background [18, 19].

The Maxwells equations governing electromagnetic fields in a dielectric medium are given as follows:

$$\vec{\nabla}.\vec{D} = 4\pi\rho \tag{1.2}$$

$$\vec{\nabla}.\vec{B} = 0 \tag{1.3}$$

$$\vec{\nabla} \times \vec{E} = -\frac{1}{c}\frac{\partial \vec{B}}{\partial t} \tag{1.4}$$

$$\vec{\nabla} \times \vec{B} = \frac{4\pi}{c}\vec{J} + \frac{1}{c}\frac{\partial \vec{E}}{\partial t} \tag{1.5}$$

where c is the velocity of light in vacuum, $\vec{E}$ and $\vec{B}$ are the electric and magnetic fields, $\vec{D}$ is the electric displacement vector. ρ and $\vec{J}(= -n_e e\vec{v})$ are the charge and current densities due to free electrons, related through the equation of continuity

$$\frac{\partial \rho}{\partial t} + \vec{\nabla}.\vec{J} = 0 \tag{1.6}$$

A characteristic frequency of plasma is the frequency of electron plasma oscillation $\omega_{pe} = (4\pi n_e e^2/m_e)^{1/2}$ where n_e, e and m_e are electron density, charge and mass respectively. The wave equation governing the propagation of electromagnetic waves in plasmas can be obtained from Maxwells equations as

$$\nabla^2\vec{E} - \vec{\nabla}\left(\vec{\nabla}.\vec{E}\right) - \frac{1}{c^2}\frac{\partial^2 \vec{E}}{\partial t^2} = \frac{4\pi}{c^2}\frac{\partial \vec{J}}{\partial t} \tag{1.7}$$

The motion of a charged particle in plasma can be described by the Lorentz force equation

$$\frac{d\vec{p}}{dt} = -e\vec{E} - \frac{e}{c}\vec{v} \times \vec{B} \tag{1.8}$$

Neglecting $\vec{v}.\vec{\nabla}v$ and $\vec{v} \times \vec{B}$ as products of smaller quantities, the above equation can be reduced to

$$\frac{\partial \vec{v}}{\partial t} = -\frac{e}{m_e}\vec{E} \tag{1.9}$$

Thus, for current density we can have

$$\frac{\partial \vec{J}}{\partial t} = -n_0 e \frac{\partial \vec{v}}{\partial t} = \frac{\omega_{pe}^2}{4\pi} \vec{E} \tag{1.10}$$

Hence,

$$\vec{J} = \frac{i\omega_{pe}^2}{4\pi\omega} \vec{E} = \sigma \vec{E} \tag{1.11}$$

where $\sigma = i\omega_{pe}^2/4\pi\omega$ is the high frequency conductivity of the plasma. $\vec{v}$ and $\vec{p}$ are the electron velocity and momentum respectively.

Taking $\vec{\nabla}.\vec{E} = 0$ and using Eqn. 1.10 in 1.7, the dispersion relation for electromagnetic waves in a plasma can be obtained as

$$\omega^2 = \omega_{pe}^2 + k^2 c^2 \tag{1.12}$$

The refractive index of the plasma can be written as $\eta(= ck/\omega) = \epsilon^{1/2}$ where $\epsilon = 1 - \omega_{pe}^2/\omega^2$ is defined as the dielectric function of the plasma. From Eqn. 1.12 it can be concluded that k becomes imaginary for $\omega < \omega_{pe}$. Thus, ω_{pe} is the minimum frequency for propagation of a light wave through a plasma. Since, the electron characteristic response time is ω_{pe}^{-1}, the electrons shield out the electromagnetic wave for $\omega < \omega_{pe}$. Hence, $\omega = \omega_{pe}$ can be referred to as the condition for electromagnetic wave propagation in plasmas. The density corresponding to this frequency is termed as the critical density $n_c = m_e\omega^2/4\pi e^2$. A plasma having density less than the critical density is termed as an underdense plasma and if it is more than the critical density, it is termed as an overdense plasma.

The electron motion becomes relativistic under the influence of laser fields that exceed 10^{11} V cm^{-1}, which results in the relativistic increase of mass. At relativistic laser intensities, the laser magnetic field also plays an important role in electron motion and hence the $\vec{v} \times \vec{B}$ term in the Lorentz force equation becomes important. For $a_0 << 1$ the laser-plasma interaction lies in the mildly relativistic regime and for $a_0 \geq 1$ the interaction lies in the highly relativistic regime where $a_0 = eE_0/m_e\omega c$ is the normalized laser vector potential. a_0 is related to the peak laser intensity I as $a_0 = 8.544 \times 10^{-10}\sqrt{I\lambda}$ where λ is the laser wavelength. Thus, for $a_0 \simeq 1$ and $\lambda = 1\mu m$, the laser intensity would correspond to $I \sim 10^{18}$ W cm^2. At this intensity,

the electron mass begins to change significantly as compared to the electron rest mass. The electron plasma frequency thus gets modified as $\omega_{pe} = (4\pi n_e e^2/m_e\gamma)^{1/2}$ where $\gamma = 1/\sqrt{1 - v^2/c^2}$ is the relativistic factor. The relativistic electron momentum can be written as $\vec{p} = \gamma m_e \vec{v}$.

1.2 The Ponderomotive Force

Highly intense electromagnetic waves such as laser beams or high-powered microwaves can exert very high radiation pressure. This high radiation pressure gets coupled to the charged particles and give rise to a force commonly known as the "ponderomotive force" [18–20]. The expression for ponderomotive force can be deduced by considering the motion of an electron in the oscillating electric and magnetic fields of an electromagnetic wave.

The wave electric field can be written as

$$\vec{E} = \vec{E}_0(\vec{r})cos\omega t \tag{1.13}$$

where $\vec{E}_0(\vec{r})$ accounts for the spatial dependence.

In the first order, the $\vec{v} \times \vec{B}$ term can be neglected in Eqn. 1.8 and $\vec{E}$ can be evaluated at the initial position $\vec{r}_0$. Thus, considering $\vec{v}_1$, $\vec{r}_1$ and $\vec{B}_1$ as the first order values, we can write

$$m\frac{d\vec{v}_1}{dt} = -e\vec{E}\,(\vec{r}_0) \tag{1.14}$$

$$\vec{v}_1 = -\frac{e}{m\omega}\vec{E}_0 sin\omega t = \frac{d\vec{r}_1}{dt} \tag{1.15}$$

$$\delta\vec{r}_1 = \frac{e}{m\omega^2}\vec{E}_0 cos\omega t \tag{1.16}$$

Expanding $\vec{E}\,(\vec{r})$ about $\vec{r}_0$ towards second order, we have

$$\vec{E}\,(\vec{r}) = \vec{E}\,(\vec{r}_0) + \left(\delta r_1 \cdot \vec{\nabla}\right)\vec{E}|_{\vec{r}=\vec{r}_0} + \cdots \tag{1.17}$$

Including the $\vec{v}_1 \times \vec{B}_1$ term where $\vec{B}_1$ can be obtained from the Maxwell's equation as

$$\vec{B}_1 = -\frac{c}{\omega}\vec{\nabla} \times \vec{E}_0|_{\vec{r}=\vec{r}_0} sin\omega t \tag{1.18}$$

in Eqn. 1.8, the second order part can be written as

$$m\frac{d\vec{v}_2}{dt} = -e\left[\left(\delta r_1 \cdot \vec{\nabla}\right)\vec{E} + \vec{v}_1 \times \vec{B}_1\right] \tag{1.19}$$

Using Eqns. 1.16, 1.17 and 1.18 in Eqn. 1.19 and averaging over time, we have

$$m\left\langle\frac{d\vec{v}_2}{dt}\right\rangle = -\frac{e^2}{m\omega^2}\frac{1}{2}\left[\left(\vec{E}_0 \cdot \vec{\nabla}\right)\vec{E}_0 + \vec{E}_0 \times \left(\vec{\nabla} \times \vec{E}_0\right)\right] \tag{1.20}$$

Using the identity

$$\vec{E}_0 \times \left(\vec{\nabla} \times \vec{E}_0\right) = \frac{1}{2}\vec{\nabla}E_0^2 - \left(\vec{E}_0 \cdot \vec{\nabla}\right)\vec{E}_0 \tag{1.21}$$

in the above equation, the expression for the effective nonlinear force on a single electron can be obtained as

$$\vec{f}_{NL} = -\frac{1}{4}\frac{e^2}{m\omega^2}\vec{\nabla}|E_0|^2 \tag{1.22}$$

Multiplying the force per unit volume with electron plasma density n_e, one can obtain the expression for ponderomotive force for a collisionless plasma as

$$\vec{F}_p = n_e\vec{f}_{NL} = -\frac{\omega_{pe}^2}{16\pi\omega^2}\vec{\nabla}|E_0|^2 \tag{1.23}$$

1.3 Laser-driven electron acceleration

Particle acceleration is one of the important and interesting areas of research due to its wide range of applications in nuclear fusion, material science, cancer therapy and many more. Laser-driven plasma-based accelerators were originally proposed three decades ago by Tajima and Dawson [5]. Plasma based accelerators are of great interest because of their ability to sustain extremely large acceleration gradients. The acceleration gradients in conventional radio-frequency (rf) linear accelerators (linacs) are currently limited to $\sim$ 100 MV/m, partly due to breakdown that occurs on the walls of the structure. Ionized plasmas can however sustain high amplitude electron plasma waves. For example, a plasma density of 10^{18} cm^{-3} yields an acceleration gradient of $\sim$ 96 GV/m which is approximately three orders of magnitude greater

than that observed in conventional linacs. Accelerating gradients on the order of 100 GV/m have been inferred in plasma based accelerator experiments [21, 22]. Moreover, plasma based accelerators are highly compact and inexpensive as compared to the large conventional accelerators. For example, the largest and the most expensive particle accelerator in the world such as the Large Hadron Collider (LHC) at CERN has a circumference of about 27 km [23], whereas a plasma accelerator can be placed on a table top.

Electrons can be a accelerated via. various mechanisms in a plasma based accelerator. In the laser wakefield accelerator (LWFA) [5, 24, 25] mechanism, a single, short ($\leq$ 1ps), high-intensity ($\geq 10^{17}$ W/cm^2) laser pulse can drive a high amplitude plasma wave. As an intense laser pulse propagates through a underdense plasma ($\omega_{pe}^2/\omega^2 \ll 1$), the ponderomotive force associated with the laser pulse envelope, $\vec{F}_p \sim \vec{\nabla} a_0^2$ expels electrons from the region of the laser pulse. The ions remain stationary due to their large mass and thus a charge separation region is created. The electrons tend to come back to their equilibrium position due to the coulomb force of the charge separation region. A plasma wave is thus generated behind the laser pulse. If the length scale L_z of the axial gradient in the pulse profile is approximately equal to the plasma wavelength, $L_z \sim \lambda_{pe}$, the ponderomotive force excites large amplitude plasma waves (wakefields) with phase velocities approximately equal to the laser pulse group velocity. When an electron bunch gets properly injected into the wakefield region, it co-propagates with the laser wakefield and gets accelerated to relativistic energies [26]. Experimental evidence of electrons accelerated via. LWFA mechanism was demonstrated for the first time by Hamster et al. [27].

In the plasma beat wave accelerator (PBWA) [28, 29], two long laser pulses of frequencies ω_1 and ω_2 are used to resonantly excite a plasma wave such that the difference is equal to the plasma frequency ($\Delta\omega \equiv \omega_1 - \omega_2 \simeq \omega_{pe}$). The idea of excitation of a plasma wave by the beating of two laser pulses was proposed for the first time by Rosenbluth et al. [28] and the concept was carried forward by Tajima and Dawson [5] as an alternative to the LWFA since compact, ultrashort pulse, ultrahigh power laser technology [30, 31] was not available in 1979. Laser pulse of intensities $\sim 10^{14} - 10^{16}$ W/cm^2 and long pulse duration ($\sim$100 ps) should be used in order to resonantly excite large amplitude plasma waves [32].

Forslund et al. [33] showed the generation of plasma beat wave using two collinear laser beams for the first time in their 2D-PIC simulations. Clayton et al. [34] have experimentally observed the excitation of a relativistic plasma wave using two copropagating CO_2 laser beams having a difference in frequency equal to the plasma frequency. Kitagawa et al. [35] have observed the acceleration of background plasma electrons up to energies more than 10 MeV in the PBWA mechanism. Clayton et al. [36] and Amiranoff et al. [37] have reported the acceleration of an externally injected electron bunch in PBWA experiments. Tochitsky et al. [38] have reported the energy gain of injected electrons due to achievement of extended laser-plasma interaction lengths through plasma-channel formation in PBWA experiments. Shvets et al. [39] have reported an analytical investigation on the parametric excitation of plasma waves by counterpropagating lasers.

In the self-modulated laser wakefield accelerator (SM-LWFA) [40–42], the laser pulse envelope gets modulated as it propagates through the underdense plasma. In the self-modulated regime, it is required that (i) the laser pulse length should be longer than the plasma wavelength, $L > \lambda_{pe}$ and (ii) the laser power should be greater than the power required for optical guiding of the laser pulse, $P > P_c$. Here, $P_c = 17(\omega/\omega_{pe})^2$ GW is the critical power required for relativistic optical guiding. The long laser pulse undergoes Forward Raman Scattering (FRS) and gets decayed into Stokes and anti-Stokes waves and a relativistic plasma wave. When the Stokes and anti-Stokes waves become sufficiently intense, they beat with the pump wave and modulate the envelope of the laser electric field amplitude. The plasma wave traps the electrons and accelerate them to relativistic energies. Enhanced electron acceleration is achieved in the SM-LWFA regime due to its several advantages. (i) The SM-LWFA is achieved at comparatively higher densities, hence high amplitude wakefield is generated. (ii) As $P > P_c$, the laser gets focussed to higher intensity which leads to an increase in the wakefied amplitude. (iii) The wakefield gets resonantly excited by a train of pulses and is thus stronger as compared to LWFA regime. (iv) Due to relativistic optical guiding, the laser pulse propagates up to several Rayleigh lengths which causes an increase in the accelerating length. The disadvantages of the SM-LWFA regime are (i) at higher densities, the laser pulse group velocity decreases which may cause the electrons to get dephased from the wakefield and hence reducing the

accelerating length (ii) the energy spectrum gets broadened due to continual trapping and short electron dephasing lengths as compared to the laser propagation lengths and (iii) the modulated phase structure gets diffracted eventually [43]. A schematic diagram of the acceleration mechanisms discussed so far is shown in Fig. 1.1.

Krall et al. [44] in their fluid simulations have illustrated the properties of the electrons accelerated in the SM-LWFA mechanism. The role of FRS in the acceleration of electrons was reported for the first time by Joshi et al. [40] in the experiments done by using a 700 ps long CO_2 laser pulse at intensity 10^{15} W/cm^2 interacting with a thin carbon foil producing 1.4 MeV electrons. Coverdale et al. [45] for the first time have experimentally observed the generation of plasma wave which leads to the generation of Stokes and anti-Stokes lines in the frequency spectrum of the laser pulse in the high-density self-modulated regime. Modena et al. [46] have experimentally reported the acceleration of electrons up to 44 MeV from the breaking of relativistic plasma waves due to FRS. An intermediate regime between standard and SM-LWFA was demonstrated in the experiments and simulations reported by Malka et al. [22] by using a laser pulse longer than the plasma wavelength. The laser pulse undergoes significant self-steepening in this regime resulting in enhanced plasma wave generation.

Another regime of acceleration is operated at high intensity limit ($a_0^2 \geq 1$), where all the plasma electrons are completely expelled from the vicinity of the laser propagation axis. An ion cavity is formed which is surrounded by a thin layer of expelled electrons. This high-intensity regime is referred to as the "blow-out", "bubble" or "cavitation" regime. In addition to electron cavitation, a fraction of the plasma electrons are self-trapped in the ion cavity and are accelerated to high energies [47–49]. Acceleration of electrons upto 40 GeV for a fraction of the electrons in the tail of the bunch has been observed in this regime [50].

Experimental results reported on laser-plasma based accelerators have shown the generation of acceleration gradients > 100 GV/m producing electron bunches with energies > 100 MeV and charge > 1nC [46, 51, 52]. However, these energetic electron bunches have a large energy spread with an exponential energy distribution with major number of electrons at low energies and a few electrons at high energies along the long exponential tail. Experimental results reported over the past decade show the

generation of quasi-monoenergetic electron beams having narrow energy spread. Leemans et al. [53] have demonstrated the generation of quasi-monoenergetic electron beams with energy about 1 GeV by 40 TW peak power laser pulses using preformed plasma channel from capillary discharge waveguides as reported in their experimental results. Clayton et al. [54] have experimentally demonstrated the generation of electron beams > 1 GeV using 200 TW laser pulses from nonpreformed plasmas. Recent advances in laser technology has made the availability of petawatt class lasers. Wang et al. [55] have experimentally demonstrated the generation of energetic electron beams up to energy 2 GeV from nonpreformed plasmas by petawatt class lasers using a 7 cm long glass cell. Kim et al. [56] have demonstrated the production of 3 GeV electron beams using a dual gas jet system of 1.4 cm. Leemans et al. [57] have reported the experimental results with supported numerical modelling on the production of electron beams with energy up to 4.2 GeV having 6% rms energy spread with 6 pC charge and 0.3 mrad rms divergence from a 9-cm-long capillary discharge waveguide by using laser pulses with peak power up to 0.3 PW.

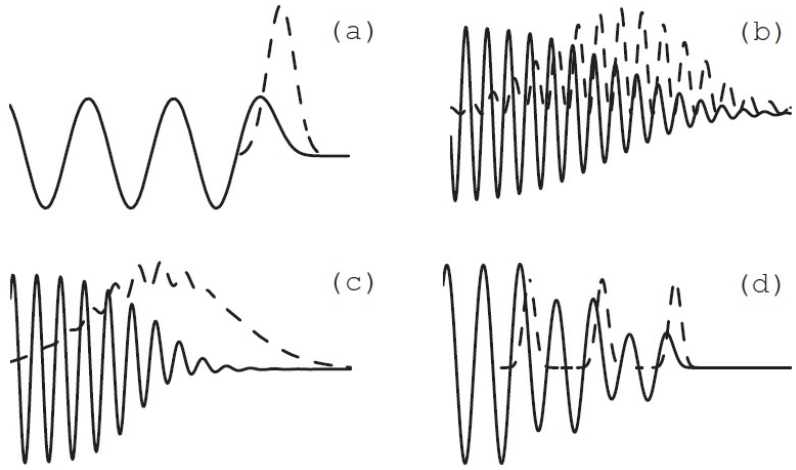

Fig. 1.1: Schematic diagram of (a) LWFA, (b) PBWA, (c) SM-LWFA and (d) resonant laser pulse train. The excited plasma wave potentials and laser intensity envelopes moving towards right are represented by the solid and dashed lines respectively [43].

1.4 Hot electron generation

Hot electrons play a fundamental role in laser-driven photonuclear physics and fast ignition in fusion targets. Moreover, acceleration of protons and heavier ions are

driven by the hot electrons. Hot or fast electrons are generated when an intense laser interacts with an overdense plasma. Since, the laser pulse cannot propagate in an overdense plasma, the pulse energy gets absorbed via. various absorption mechanisms. The laser pulse energy gets transported to the electrons which makes them move with relativistic velocities. The energy of hot electrons which may also be termed as the "ponderomotive" energy [58] is the cycle-averaged oscillation energy in the laser electric field in vacuum can be written as

$$\mathcal{E}_{eh} = m_e c^2(\gamma - 1) = m_e c^2(\sqrt{1 + a_0^2/2} - 1) \tag{1.24}$$

If the laser is p-polarized and is obliquely incident on a plasma at an angle θ having a density gradient $\vec{\nabla} n_e$, such that there is component of the laser electric field which satisfies the condition $\vec{E}.\vec{\nabla} n_e \neq 0$, resonant plasma oscillations are driven at the critical layer which generates hot electrons as shown in Fig. 1.2. The laser gets turned at the electron density $n_e = n_c cos^2\theta$ which is less than the critical density for $\theta > 0$. The electric field component of the incident laser generates a standing wave pattern which causes electron oscillations in a direction parallel to the density gradient. These oscillations create charge density fluctuations which can be resonantly enhanced by the plasma. Thus, the laser transfers a part of its energy to the electrons and generates an electron plasma wave. This absorption process is termed as resonance absorption. The density scale length $L_s = n_e/|\vec{\nabla} n_e|$ plays an important role in this absorption mechanism as the driving force is evanescent in the resonance region.

In case of a plasma with sharp boundary $L_s \ll \lambda$, electrons are driven from the strong field region to the evanescence region so in a time shorter than $2\pi/\omega$ so that the cycle average $-e\langle\vec{E}.\vec{v}\rangle$ does not cancel out. Thus, laser absorption and electron heating may occur as the electron motion is not adiabatic. High-intensity and short pulse duration lasers favours electron heating as the hydrodynamic expansion does not have sufficient time to wash out the sharp density gradients. In sharply edged plasmas, hot electrons can be generated through an absorption mechanism termed as "vacuum heating" [59]. In this mechanism, the electric field of an obliquely incident p-polarized laser drags the electrons out of the plasma surface and as the electric field reverses its direction at later times, the electrons go back into the plasma again,

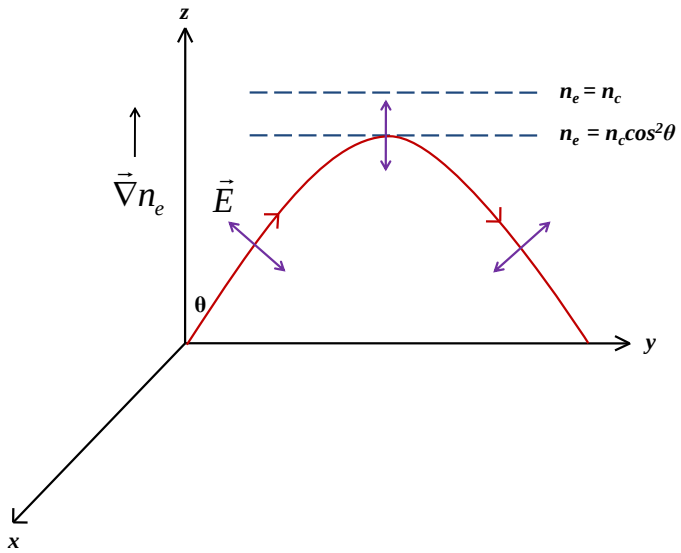

Fig. 1.2: Schematic diagram of electron heating via resonance absorption process [19].

which results in an efficient heating of electrons.

In case of *s*-polarization or normal incidence, there is no laser electric field component normal to the plasma surface. At high intensities the magnetic force becomes important which may drive electron oscillations along the direction of the density gradient even when the laser is normally incident. The magnetic force oscillates at 2ω which leads to the generation of hot electron bunches at twice the laser period. This mechanism of absorption is commonly named as "$\vec{J} \times \vec{B}$" heating [60].

In case of a normally incident circularly polarized laser, the oscillating component of the laser electric field normal to the plasma surface vanishes. Hence, electron heating may get suppressed in this case. The electric field for a circularly polarized laser propagating along $\hat{x}$ can be written as [61]

$$\vec{E}_{cp} = E_{cp}(x)[sin(\omega t)\hat{y} + cos(\omega t)\hat{z}] \tag{1.25}$$

The ponderomotive force for a circularly polarized laser is given as

$$\vec{F}_p = -\frac{m_e c^2}{4}\frac{\partial}{\partial x} a_{cp}^2(x)\hat{x} \tag{1.26}$$

where $a_{cp}(x) = eE_{cp}(x)/m_e\omega c$ is the normalized electric field amplitude, m_e, ω and c

have their usual meanings.
Thus, it can be observed that for circular polarization and normal incidence, the oscillating component in the ponderomotive force vanishes. The radiation pressure thus has a steady effect for circularly polarization which can push the plasma surface forward while the electron heating is quenched.

In most of the high-intensity laser-plasma experiments, the main short pulse is preceded by a prepulse which causes the formation of a preplasma. The preplasma expands which reduces the density and increases the scale length. Thus, the interaction does not occur with a sharp boundary solid density plasma. However, the density profile may get steepened at the critical surface ensuring the interaction to occur with a sharp density profile having a lower density variation in comparison with the solid density. The electrons may get accelerated in the underdense region of the preplasma which might lead to an additional increase in electron energy [62].

The transport of hot electrons in high density plasma or solid density can be characterized by the high current density and the self-generated magnetic fields. The current density $\vec{j}_h = -en_n\vec{v}_h$ generated due to hot electrons at the target front surface my reach values up to $j_h \sim -en_c c \simeq 4.8 \times 10^{12}$ A/cm^2 which corresponds to a total current of $\sim$ 15 MA over circular spot of 10 μm radius. This high forward current should be neutralized by a return current $\vec{j}_r$ composed of cold electrons such that $\vec{j}_h + \vec{j}_r \simeq 0$ in order to prevent the generation of electric field due to charge imbalance or the generation magnetic field due to free flowing $\vec{j}_h$ which would be strong enough to stop the hot electrons for further penetration into the solid density region [63, 64].

Hot electrons generated in relativistic laser-plasma interactions play an important role in the Fast Ignition (FI) scenarios in the Inertial Confinement Fusion (ICF) scheme [65] as shown in Fig. 1.3. At the first stage, a long pulse of intensity $\approx 10^{14}$ W/cm^2 compresses the target and a high density core is created. The core is surrounded by an ablation cloud consisting of an overdense plasma covered by an underdense plasma. At the second stage, a high-intensity pulse of duration 100 ps and intensity $\approx 10^{14}$ W/cm^2 creates a plasma channel which behaves as a waveguide for the ignitor beam. At third stage, the ignitor beam of 5 ps pulse duration and intensity $\approx 10^{20}$ W/cm^2 is stopped at the overdense plasma and hot electrons are generated. At fourth stage, these hot electrons propagate to the high-density core

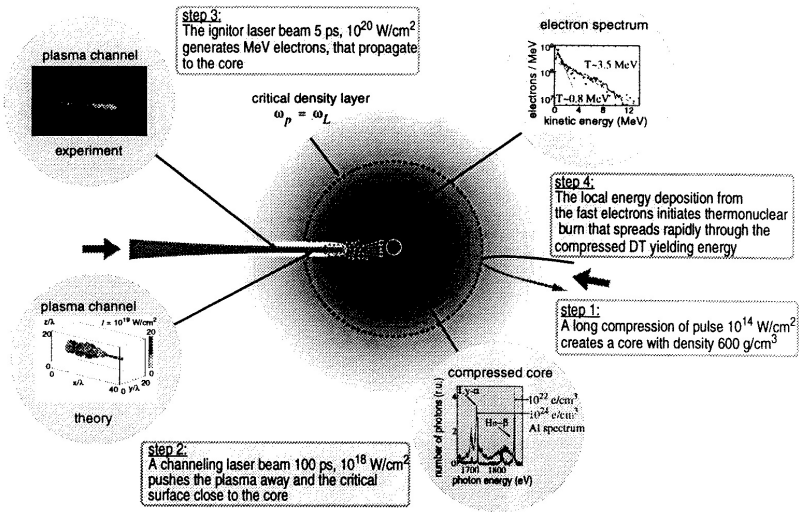

Fig. 1.3: Schematic diagram of the fast ignition in inertial confinement fusion after the termination of the pulse which drives the implosion and compresses the fuel [65].

and ignite it.

1.5 Laser-driven ion acceleration

The generation of high energetic protons have been an interesting area of research in the field of laser-plasma interactions due to its wide range of applications in fast ignition scenarios [66], proton radiography [67], proton imaging techniques [68], nuclear physics [69], cancer therapy [70, 71], as well as in astrophysics [72].Several experiments done before the year 2000 by irradiating high-intensity lasers on targets such as thick solid foils [73, 74], gas jets [75, 76] and submicrometric clusters [77, 78] have lead to the generation of ions having energies up to several MeVs. However, the energetic ions generated in all such experiments had a common disadvantage of isotropic ion emission resulting in low brilliance which made them quite unsuitable for their use as ion accelerators for applications. In the year 2000, Clark et al. [79], Maksimchuk et al. [80] and Snavely et al. [81] have reported the generation of protons having energies 1.5 MeV, 18 MeV and 58 MeV respectively in their experiments done by irradiating either solid metallic or plastic (CH) targets with high-intensity laser pulses. These energetic protons were detected at the rear side of the target opposite to the front side at which the laser is irradiated and were emitted in the form of a collimated proton beam along the target normal direction. The mechanism behind

the acceleration of protons from the target rear side was introduced by Wilks et al. [82] in their target normal sheath acceleration (TNSA) model. In this mechanism, a high-intensity laser irradiates the solid target and ionizes the front surface and thus generates hot electrons (the electron cloud) as shown in Fig. 1.4. The plasma starts to expand towards the laser and the hot electrons penetrate through the target getting inhibited by an internal electric field. The hot electrons cross the rear side boundary and attempt to escape in vacuum inducing a strong sheath electric field which ionizes atoms in the surface layer and accelerates the ions in the target normal direction.

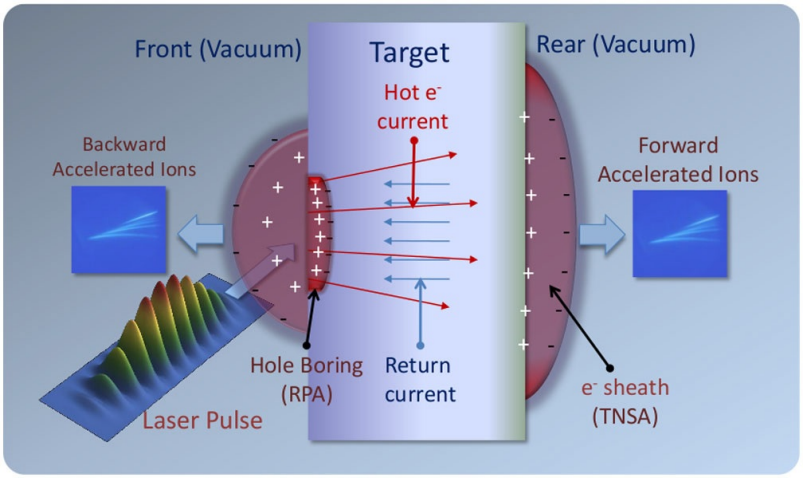

Fig. 1.4: Schematic diagram of ion acceleration by TNSA mechanism [62].

The plasma expansion can be explained by a simple model assuming a one-dimensional (1D) expansion of the plasma into vacuum at the rear side of the plasma. The electrons are assumed to be in isothermal equilibrium and the electron density is given by the Boltzmann relation. If quasineutrality ($n_e = Zn_i$) is assumed, neglecting electron inertia the ion continuity equation and equation of motion can be written as [82]

$$\frac{\partial n_i}{\partial t} + \frac{\partial (n_i \vec{v}_i)}{\partial x} = 0 \tag{1.27}$$

and

$$\frac{\partial \vec{v}_i}{\partial t} + \vec{v}_i \frac{\partial \vec{v}_i}{\partial x} = -\frac{Ze}{m_i} \frac{\partial \phi}{\partial x} \tag{1.28}$$

where m_i is the ion mass, n_i and $\vec{v}_i$ are the ion density and velocity respectively. ϕ

is the electrostatic potential satisfying Poisson's equation

$$\nabla^2\phi = 4\pi e(n_e - Zn_i) \tag{1.29}$$

Assuming that n_i and $\vec{v_i}$ have have a space and time dependence of the form $\zeta = x/t$ one can obtain the solutions for n_i and $\vec{v_i}$ as

$$n_i = n_{io} exp\left(-1 - \frac{x}{C_s t}\right) \tag{1.30}$$

and

$$\vec{v_i} = C_s + \frac{x}{t} \tag{1.31}$$

where $C_s = \sqrt{ZT_e/m_i}$ is the ion acoustic speed and T_e is the electron temperature. The electric field $\vec{E_s}$ which accelerates the ions can be calculated from the electron equation of motion

$$n_e e E_s = -\frac{\partial p}{\partial x} \tag{1.32}$$

The accelerating field can thus be written as

$$E_s = \frac{T_e}{eC_s t} \tag{1.33}$$

As noted for the self-similar solution, we can write

$$E_s = \frac{T_e}{eL_s} \tag{1.34}$$

where L_s is the local plasma scale length which represents the typical spatial expansion of the sheath.

Hegelich et al. [83] in their experiments have shown that heavier ions of several different species can be accelerated on a longer time scale provided number of protons accelerated are not high enough which would balance the charge of escaping hot electrons. Moreover, the acceleration is enhanced if the impurity protons are removed before the interaction by preheating the target. Snavely et al. [81] in their experiments with a wedge target have reported the emission of two separate proton beams along two different directions normal to the two rear surfaces of the wedge target. Experimental observations on interaction of ultraintense laser pulses

with preformed or nonpreformed plasmas reported by Mackinnon et al. [84] show the dependence of the plasma scale length at the target rear side on the peak and mean energies of the proton beam. They have observed the emission of high energetic proton beams from the unpurturbed rear surface whereas no energetic proton beams were emitted in case of a target having longer scale length in the ion density at the target rear side. Allen et al. [85] in their experiments have reported that the removal of contaminants on the target rear side of Au foils strongly reduced the total yield of energetic protons whereas removal of contaminants from the target front side had no significant effect in the acceleration. Cowan et al. [86] have reported the observation of modulations in the proton beam which is produced due to structuring of the target rear surface. Such experiments strongly provide an evidence that the ions are accelerated mainly from the target rear side. The properties such as the spatial and angular characteristics of the ion beams produced due to TNSA has been studied in several experiments. A number of researchers such as Fuchs et al [87], Borghesi et al. [88] and Zeil et al. [89] have studied the characteristics and maximum energy cutoff of the TNSA ion beams in their experiments for a wide range of laser and target parameters. Experimental observations reported by Snavely et al. [81] and Fuchs et al. [90] have shown that the ion beams produced from conducting targets have much smoother beam profiles with a sharp boundary than those produced from dielectric targets. Structured beam profiles can also be produced if their is a roughness in the target rear surface which may result in randomized local orientations of the ions as reported by Roth et al. [91]. A modulation in the proton beam angular distribution can be produced by microstructuring the target rear surface [86].

The effect of ion acceleration on target thickness was experimentally investigated by Mackinnon et al. [84] and they have observed that the peak proton energy increases from 6.5 to 24 MeV on decreasing the thickness of the Al foil target from 100 to 3 μm. Thus, it can be understood that an increase in the target thickness reduces the mean hot electron density at the surface which lowers the peak proton energy. Kaluza et al. [92] have experimentally reported the effect of laser prepulse due to amplified spontaneous emission (ASE) on proton acceleration from thin Al foils of different thicknesses. They have observed the existence of an optimal value for the target thickness at which maximum proton energy is obtained. The optimum

thickness is observed to be strongly dependent on the prepulse duration. Neely et al. [93] have experimentally reported the observations on experiments with ultrathin Al targets of 20 nm thickness using high contrast laser pulse of duration 33 fs. In such cases, refluxing and concentration of hot electrons occur within a small volume which establishes a strong electric field resulting in high ion energies.

Target geometry and shape effects play a significant role in the acceleration process. Mass-limited-targets which have limited lateral transverse dimensions helps in the refluxing and concentration of hot electrons occur within a small volume which establishes a strong electric field resulting in high ion energies. Numerical simulations by Piskal et al. [94] have shown that using a target of reduced surface can result in high hot electron density at the target rear side which leads to the formation of strong accelerating electric fields. Buffechoux et al. [95] have experimentally observed that reduced transverse dimensions may result in the reflection of the hot electrons from the lateral edges of the target at time scales comparable to the acceleration. Such transverse refluxing of hot electrons result in the formation of dense and homogeneous electron sheath across the target-vacuum interface which leads to a significant increase in the maximum proton energy as well as in the laser-to-ion conversion efficiency. Gaillard et al. [96] have recently reported experimental results on an increase in the maximum energy cutoff up to 67.5 MeV using flattop hollow microcones [97] as targets. These targets are the modified version of the conical targets used in the fast ignition experiments. The laser pulse gets focused as it moves by interacting with the walls of the cone and finally interacts with the flattop section. This results in an increase in the number of hot electrons which increases the maximum proton energy.

At ultra high intensities ($\geq 10^{20}$ W/cm^2), the effect of radiation pressure becomes dominant on driving the particle motion and the acceleration. The use of circularly polarized laser helps in the generation of quasimonoenergetic ion bunches and hence increases the efficiency of ponderomotive ion acceleration [98, 99]. For a plane monochromatic wave of intensity I normally incident on the plane surface of the medium at rest, the radiation pressure is given by

$$P_{rad} = (1 + R - T)\frac{I}{c} = (2R + A)\frac{I}{c} \tag{1.35}$$

where R, T and A are reflection, transmission and absorption coefficients (with

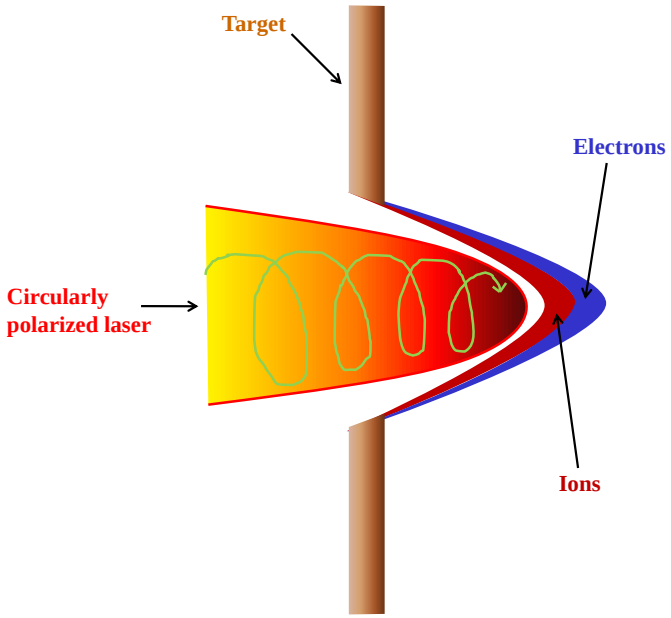

Fig. 1.5: Schematic diagram of ion acceleration by RPA mechanism [100].

$R + T + A = 1$). These coefficients are defined as a function of the refractive index and thus of the wave frequency [101].The radiation pressure is related to the steady ponderomotive force of the electromagnetic wave. Since, the ponderomotive force is inversely proportional to the particle mass, it acts effectively on the electrons. When an intense laser pulse is incident normally on an overdense plasma surface, the laser ponderomotive force pushes the plasma electrons inwards and creates a charge separation region. The electrostatic field of this region acts on the ions and accelerates them as shown in Fig. 1.5.

In case of thick targets, the radiation pressure acceleration (RPA) falls under the Hole boring (HB) regime. In this regime, the laser pulse ponderomotive force pushes the electrons which results in the formation of a steep density rise in front of the laser pulse. The electrons reflect the laser pulse and move forward leaving the ions behind. Thus a charge separation zone is created and the ions are accelerated in the forward direction by the electrostatic field. The ion density peak thus follows the electron density peak and a double layer structure is created which is most popularly known as the "laser piston" [102, 103] as shown in Fig. 1.6.

It is assumed that electron and ion heating doesn't occur in the interaction zone. The laser light gets Doppler downshifted in the reference frame of the piston moving

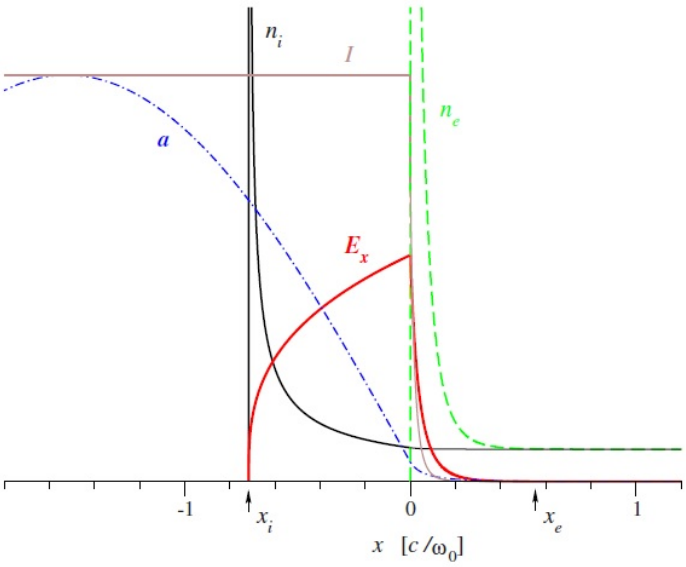

Fig. 1.6: Double layer of the laser piston formed by the radiation pressure. a is the laser field amplitude (blue dotted-dashed), I is the laser intensity (brown thin solid), n_e is the electron density (green dashed), $\vec{E}_x$ is the longitudinal electrostatic field (red thick solid), n_i is the ion density (black solid). Ion charge separation layer (x_i,0) is situated in front of electron sheath (0,x_e) [102].

with velocity $\vec{v}_{pist} = \beta_{pist} c$. The laser frequency in the moving frame ω' and that in the laboratory frame ω are related to each other by the Lorentz transformation as $\omega' = \omega\gamma_{pist}(1 - \beta_{pist})$ where $\gamma_{pist} = (1 - \beta_{pist})^{-1/2}$. The laser is completely reflected from the plasma and the momentum flux deposited by the photons on the moving frame is $2I'/c$. Here, I' is the laser intensity at the moving frame related to the the same at the laboratory frame I by the Lorentz transformation, $I' = I(1-\beta_{pist})/(1+\beta_{pist})$. The balancing of particle momentum flux $2n_i v_{pist}^2 m_i \gamma_{pist}$ and the radiation pressure can be written as [102]

$$\frac{2I}{c}\frac{1-\beta_{pist}}{1+\beta_{pist}} = 2n_i v_{pist}^2 m_i \gamma_{pist} \tag{1.36}$$

The piston velocity can thus be obtained as

$$\beta_{pist} = \frac{\Gamma^{1/2}}{1+\Gamma^{1/2}} \tag{1.37}$$

where

$$\Gamma = \frac{I}{m_i n_i c^3} = \frac{Z}{A}\frac{n_c}{n_e}\frac{m_e}{m_p}a_0^2 \tag{1.38}$$

where m_p is the proton mass, Z and A are the atomic and mass numbers respectively.

The ions gain energy when they get reflected by the piston. The maximum kinetic

energy per nucleon can thus be obtained as

$$\mathcal{E}_{max} = 2m_p c^2 \frac{\Gamma}{1 + 2\Gamma^{1/2}} \tag{1.39}$$

In the non-relativistic case, $\Gamma \ll 1$ and $\vec{v}_{pist} \ll c$, hence one can obtain $\vec{v}_{pist}/c \simeq \Gamma^{1/2}$ and $E_{max} \simeq 2m_p c^2 \Gamma$ [102, 104].

In case of thin targets, the acceleration falls under the light sail (LS) regime. In this regime, the foil used for acceleration is sufficiently thin. Hence, the hole boring reaches its rear surface. The laser pulse punches through and accelerates the compressed ion and electron layers, detached from the foil as a single quasineutral plasma slab. The laser pulse is further able to accelerate the ions to high energies as they are not screened by the background plasma anymore [105, 106].

Ions can also be accelerated by electrostatic collisionless shocks formed at the front side of the target in the collisionless shock acceleration (CSA) mechanism. In the frame moving at the shock velocity, the shock reflects the ions if the height of the electrostatic potential barrier Φ is such that $Ze\Phi > m_i v_{is}^2/2$, where $\vec{v}_{is}$ is the velocity of the ion component in the shock frame. Ions initially at rest acquire a velocity of $2\vec{v}_{shock}$ in the laboratory frame after being reflected by the shock front moving with the velocity $\vec{v}_{shock}$. The CSA mechanism in accelerating ions in the interaction of superintense laser pulses with overdense plasmas was first proposed by Denavit [107] and Silva et al. [108] in their particle-in-cell (PIC) simulations. Silva et al. [108] have reported the generation of shocks with high Mach numbers $M = \vec{v}_{shock}/c_s = 2 - 3$, where c_s is the local sound speed estimated using the hot electron energy as temperature i.e., $T_{eh} \simeq \mathcal{E}_{eh} = m_e c^2(\gamma - 1)$. The shocks are assumed to be driven by the laser piston generated due to radiation pressure and are generated at the target front surface with shock velocity closer to the piston velocity $\vec{v}_{pist}$.

At present, though the experimental evidence of RPA is less clear, but some of the experimental results can be interpreted using the ponderomotive acceleration model [102]. Palmer et al. [109] have reported experimental observations on acceleration of protons by an electrostatic shock driven by the radiation pressure at the target front surface. Badziak et al. [110] have reported a series of observations on the generation of high-density, $\sim$ keV energy ion pulses (plasma "blocks") from solid targets using a laser of subrelativistic intensity ($\sim 10^{18}$ W/cm^2). Akli et al. [111]

have reported on heating of solid-density matter due to the density profile steepening by shock formation induced by lasers of intensities about 5×10^{20} W/cm^2. Heing et al. [112] have reported the acceleration of ions from a mass-limited spherical target by a converging shock induced by a linearly polarized laser of intensity 10^{20} W/cm^2. Though, electron heating due to the use of linear polarization make the acceleration process complicated, the supporting PIC simulation results reported by them confirm the acceleration as HB-RPA. Esirkepov et al. [113] have reported 3D-PIC simulation results on acceleration of ions by a laser pulse of intensity 1.4×10^{23} W/cm^2 up to relativistic energies ($\sim$ 1 GeV) in the LS-RPA regime. Pegoraro et al. [114] have shown the significance of the role played by the Rayleigh-Taylor-like instabilities in the radiation pressure dominated regime. The concept of using ultrahigh-intensity lasers for achieving RPA as proposed by Esirkepov et al. [113] is still above the scope of present-day laser technology. However, RPA can still be achieved at comparatively lower intensities with a normally incident circularly polarized laser for thick targets as shown in the PIC simulations reported by Macchi et al. [100]. A number of multi-dimensional PIC simulations reported the use of flattop transverse profiles to maintain a quasi-1D geometry in order to reduce the electron heating due to transverse effects caused by inhomogeneous laser intensity distribution [106, 115, 116]. Kar et al. [117] have reported the experimental observations on the generation of energetic protons and carbon ions having narrow-band features peaked at 5-10 MeV/nucleon range by using 250 TW, subpicosecond laser pulses focussed to intensities 3×10^{20} W/cm^2. The ion energy spectra showed resemblance with the scalings according to the LS-RPA model. Heing et al. [118] have experimentally reported the difference in the energy spectra of fully ionized C^{6+} ions between linearly and circularly polarized pulses obtained by using 45 fs laser pulses at intensity $\sim 5 \times 10^{19}$ W/cm^2. Electron heating was observed to be reduced for a circularly polarized laser resulting in a pronounced peak centered at $\approx$ 30 MeV in the C^{6+} ion energy spectrum. Haberberger et al. [119] have demonstrated the generation of monoenergetic proton beams accelerated up to 22 MeV by laser-driven collisionless shocks in the interaction of a 100 ps, CO_2 laser pulse at intensity 6.5×10^{16} W/cm^2 with a hydrogen gas jet. Kim et al. [120] have reported the generation of 93-MeV proton beams by irradiating 800 nm, 30 fs circularly polarized laser pulses at intensity 6×10^{20} W/cm^2 on 15 nm thick

polymer targets and have confirmed the acceleration mechanism as radiation pressure acceleration from the obtained from the optimum target thickness, quadratic energy scaling, polarization dependence and 3D-PIC simulations.

Another acceleration mechanism which leads to the generation of GeV ions is termed as the laser break-out afterburner (BOA) acceleration [121, 122]. In this mechanism, ultrathin foils are used as targets for acceleration. The acceleration process goes through three distinct stages. In the first stage, the ultraintense laser generates hot electrons at the target front surface which moves through the target and on reaching the rear side accelerates the ions via. TNSA mechanism. A flow of electrons occurs into the laser interaction region due to the return cold current. The second stage is the enhanced TNSA stage in which the laser reheats the refluxing cold electrons to even higher energies and enhances the sheath field. Thus, more number of hot electrons are generated which move towards the rear side leading to the reduction of electron density inside the target which in turn lowers the plasma frequency ω_{pe}. Moreover, when the electrons are heated to relativistic energies, ω_{pe} gets lowered by $\sqrt{\gamma}$ and falls below ω due to relativistically induced transparency. The third stage is the "break-out afterburner" in which the plasma expands and becomes underdense to the laser and hence, the laser penetrates to the target rear side and generates a large localized longitudinal field through Buneman instability. Thus, the ions get accelerated to high energies in the form of a quasimonoenergetic ion beam.

Ions can also be accelerated effectively to high energies from near-critical and underdense plasmas such as cluster-gas targets and foams. These targets are considered to be advantageous for ion acceleration as they support the formation of plasma waveguide which can make the laser pulse move through a long distance in the plasma and generate large number of hot electrons which can create strong electric fields. Moreover, replenishable cluster targets facilitates high repetition rate of accelerated ions which are free from plasma debris and are highly collimated [124]. 2D-PIC simulations show that the energetic ions generated at the target rear side from such targets is due to the formation of a strong magnetic vortex structure. This acceleration process is known as magnetic vortex acceleration (MVA) [125, 126] as shown in Fig. 1.7. In this mechanism, the quasistatic magnetic field $\vec{B}_s$ at the rear surface

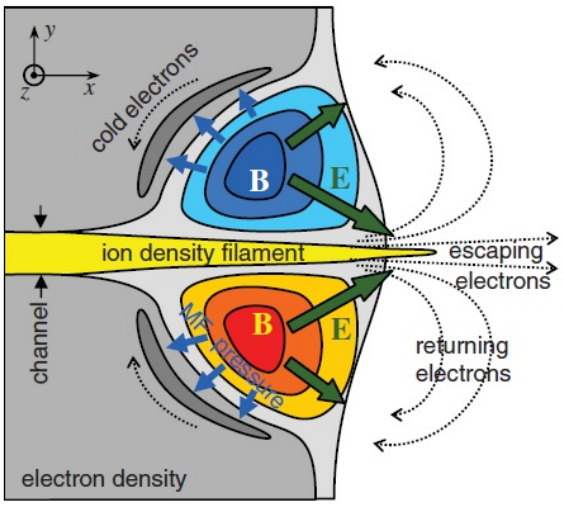

Fig. 1.7: Schematic diagram of ions accelerated by MVA mechanism [123].

enhances the accelerating electric field $\vec{E}_s \simeq \nabla B^2/8\pi e n_e$ of the electrostatic sheath which accelerates the ions via. magnetic pressure and induction effects [123, 127].

1.6 Magnetic field generation

The generation of high magnetic fields has been an active area of research since many years in the field of laser plasma interactions [128–130]. Huge magnetic field of the order of 10^8 G is generated on the interaction of an ultrashort laser pulse with a solid target [131]. The interaction of multiterawatt lasers with focused intensities of the order of 10^{19} W/cm^2 and dense solid targets generates hot electrons, which penetrate deeply into the target and excites return shielding currents. These hot electrons play a major role in fast ignition scenarios, where they transport the energy through the overdense plasma to the center of the compressed core and ignite the fuel there [132]. The energetic electrons are extremely useful in the production of ultrafast X-ray pulses [133], generation of MeVGeV protons and ions [134].

The hot electrons on propagating through the overdense plasma makes the system unstable and results in the generation of a relativistic electromagnetic two-stream instability or more commonly known as the Weibel instability [135], which is mostly responsible for the generation of quasi-static magnetic fields. Weibel in his classic paper has shown that a magnetic field perturbation can make a plasma having anisotropic temperature unstable. A purely growing magnetic field is produced by the free energy stored in electron temperature. Fried [136] gave a physical interpreta-

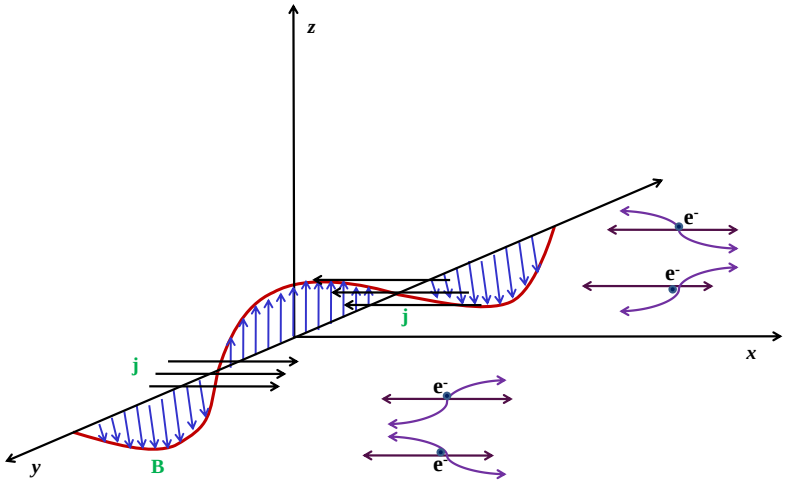

Fig. 1.8: Physical mechanism of Weibel instability induced by two counter-propagating electron beams [136].

tion of Weibel instability in presence of counterstreaming electron beams in plasmas as shown in Fig. 1.8. Due to anisotropic electron temperature, the electrons will move with a thermal velocity along $\hat{x}$ direction. Assuming an initial perturbation in the magnetic field arising from noise polarized along $\hat{z}$ and propagating along $\hat{y}$ direction, it can be speculated that the electron will get deflected by the magnetic field and will acquire a velocity along $\hat{z}$ direction which will grow with time.

Magnetic fields can also be generated in presence of non-parallel temperature and density gradients [i.e., $\partial B/\partial t = (1/n_e e)(\nabla T_e \times \nabla n_e)$]. Schloutter et al. [137] have demonstrated that the presence of non-parallel temperature and density gradients can give rise to a pressure which can swiftly move the lighter electrons against the heavy ions causing a space charge field and electron currents. Stamper et al. [138] have investigated the generation of baroclinically induced magnetic fields in context of laser-produced plasmas. A finite-sized laser beam when irradiated on a target esablishes a density gradient which is pointed inwards the solid-density target face, whereas the temperature gradient is pointed radially inward towards the laser beam axis near the edge of the laser spot as shown in Fig. 1.9. A toroidal magnetic field is generated having a scale size comparable to the laser spot which falls to zero at the laser beam axis. The radial temperature gradients are thought to be small near the middle of the laser focal spot due to usual flat intensity distribution. Thus, low magnetic fields at the center of the focal region is expected.

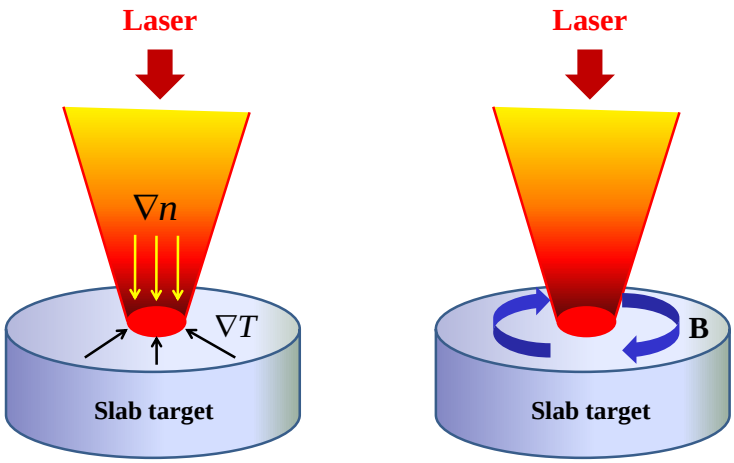

Fig. 1.9: Schematic diagram of toroidal magnetic fields generated by the $\nabla T_e \times \nabla n_e$ mechanism [138].

Magnetic fields can also be generated by the laser ponderomotive force of a nonuniform intense electromagnetic beam [139, 140]. The ponderomotive force will swiftly expel the electrons from high field intensity region to low field intensity region such that they pile up in the region of low intensity. Thus, electron currents are set up which may lead to generation of magnetic fields.

1.7 High-order harmonic generation

Harmonics generated due to the interaction of intense short pulse lasers with plasmas has been an active area of research in recent years [14]. Due to their short wavelength, harmonic generation is one of the most widely discussed areas in laser-plasma interactions as it has many applications such as the generation of attosecond pulses [141], study of material properties, biological samples etc. It can be used as a diagnostic tool for overdense plasmas since at second harmonic frequency laser can penetrate into such plasmas and may provide us information regarding various phenomena occurring therein [142–144]. Harmonics can also be used for probing of rotational dynamics of molecules [145] and also in observation of molecular structure [146]. Besides higher order harmonics serves as an excellent source of ultrashort coherent extreme ultraviolet (EUV) radiation [147–149].

Harmonics are generated effectively from gaseous targets and clusters. The intense

electric field of the laser ionizes the atom and pulls the electron away from the parent ion. As the laser electric field changes its polarity, the electron will slow down and stop at a position far away from the parent ion and then it starts getting accelerated towards the parent ion. On reaching the parent ion, the recombination occurs and a photon of energy equal to the instantaneous kinetic energy and the ionization potential of the parent atom is emitted [150]. This gives rise to the generation of higher order harmonics as observed in experiments [151].

Ionization of atoms can occur via. optical field ionization (OFI) and multi photon ionization which is determined by a parameter particularly known as Keldysh parameter Γ [152] and is defined as:

$$\Gamma = \sqrt{\frac{I_p}{2U_p}} \tag{1.40}$$

where I_p is the ionization potential and U_p is the ponderomotive potential which is the cycle-averaged quiver energy of an electron in the laser electric field. U_p is defined as:

$$U_p = \frac{e^2 E^2}{4 m_e \omega^2} \tag{1.41}$$

For $\Gamma \gg 1$, the ionization mechanism is dominated by multiphoton ionization whereas for $\Gamma \ll 1$, OFI dominates by almost instantly knocking the electrons out of the atomic levels. OFI occurs via. two different mechanisms namely tunnel ionization and barrier suppression ionization (BSI) [153]. When the laser electric field strength becomes comparable to the atomic field strength, tunnel ionization occurs. The atomic potential well gets distorted and the potential barrier is lowered causing an electron to come out freely of the atomic structure as shown in Fig. 1.10 (a). When the laser electric field is strong enough to suppress the potential barrier below the electron energy level, the electrons come out of the atomic levels through BSI mechanism as shown in Fig. 1.10 (b).

At the initial stage, McPherson et al. [154] have experimentally detected the presence of harmonic radiation by irradiating intense ultraviolet light of intensity $10^{15} - 10^{16}$ W/cm^2 on rare gases. Crane et al. [155] have experimentally reported the observation of harmonics up to 45$^{\text{th}}$ order of a 526 nm laser light in He. L'Huillier and Balcou [156] have reported the observation of harmonics using a 1-ps 1053 nm

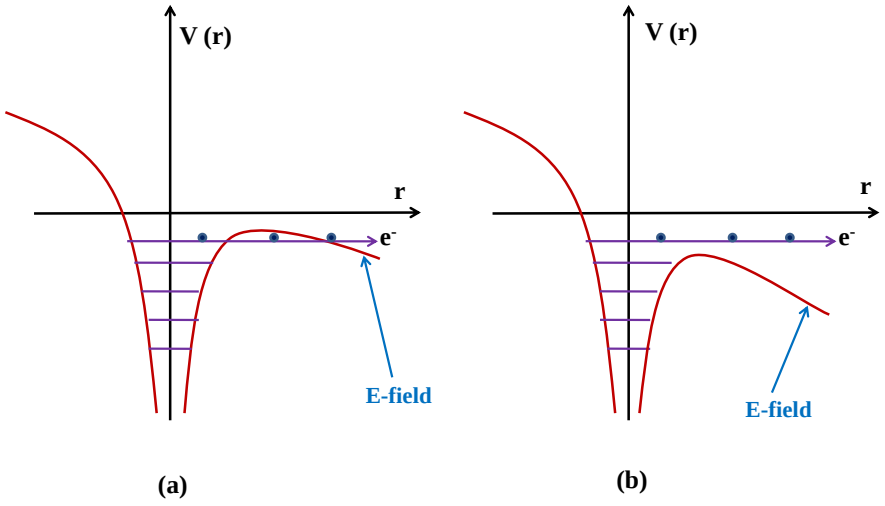

Fig. 1.10: Schematic diagram of potential-well ($V(r)$ vs r) distortion (a) tunnel ionization and (b) barrier suppression ionization (BSI) [153].

10^{15} W/cm^2 Nd:Glass laser up to 29$^{\text{th}}$ order in Xe, 57$^{\text{th}}$ in Ar and 135$^{\text{th}}$ in Ne. Macklin et al. [157] have reported the generation of harmonics up to 109$^{\text{th}}$ order below 10 nm from Ne gas excited by 800 nm Ti:Sapphire laser pulses (15 mJ, 125 fs) at intensity near 10^{15} W/cm^2. Chang et al. [158] have observed the generation of coherent soft-x-ray harmonics up to $\approx 300^{\text{th}}$ order at wavelengths down to 2.7 nm (460 eV) in He and 5.2 nm (239 eV) in Ne which is within the "water window" region of x-ray transmission. Spielmann et al. [159] have also observed the generation of harmonics at wavelengths 4.37 nm in the water window region by performing experiments with 5 fs laser pulses irradiated on a He gas jet.

Harmonics can also be generated efficiently from solid surfaces. The generation of these harmonics can be well explained by the "oscillating mirror model" [160–162]. When a short pulse laser interacts with a sharply edged overdense plasma surface, it drives the electrons back and forth of the plasma boundary. Since, the laser pulse is short, the ions can be considered as immobile and they can be treated as a fixed positive background charge. The laser gets reflected from the critical density surface. The changes in electron density profile is neglected and the electron motion is represented by the collective electron motion of the boundary of the supercritical region. This boundary represents the effective reflecting surface which undergoes an oscillatory motion and is hence termed as the "oscillating mirror". The reflecting

surface oscillates at a frequency of 2ω or a superposition of ω and 2ω. Thus, the modulation frequencies produced in the sidebands are ω and/or 2ω which represents the harmonics. Hence, both odd and even harmonics are produced. The plasma boundary should be sharply edged i.e., the plasma scale length should be short. For large scale length the oscillating reflecting surface would become indistinct which would reduce the efficiency of harmonic generation. For low intensity lasers i.e., in the non-relativistic regime ($a_0 << 1$), harmonics are generated only in the case of p-polarized lasers since, the electron motion in the direction normal to the plasma surface is absent in case of s-polarized lasers. For high intensity lasers i.e, in the relativistic regime ($a_0 \geq 1$), the electrons move in a "figure-eight-motion" as shown in Fig. 1.11. Thus, electron motion normal to the target surface occurs in case of

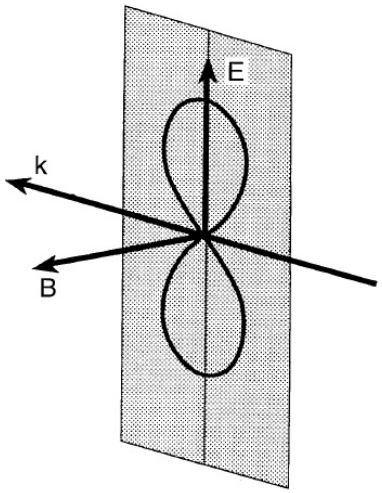

Fig. 1.11: Figure-eight-orbit of an electron in a linearly polarized plane electromagnetic wave. $\vec{E}$, $\vec{B}$ and $\vec{k}$ denote the electric field, magnetic field and the wave propagation vector respectively [160].

s-polarized lasers. Hence, in the relativistic regime, harmonics are generated in case of both p- and s-polarized lasers. However, intensity of harmonics is highest in case of p-polarized lasers. Besides "oscillating mirror" model, since the electron motion in "figure-eight-motion" is periodic, they should radiate photons which are harmonics of each other having their own unique angular distribution [160, 161, 163].

In addition to the generation of harmonics due to phase modulation by the oscillating mirror, harmonics are also generated due to a change in the electron charge density at the plasma surface. The laser induced back and forth motion of the reflecting surface causes a surplus or deficiency of electrons in the plasma boundary.

Since, the ions are considered to be stationary, an electric dipole sheet is formed at the vacuum-plasma boundary as shown in Fig. 1.12. In case of *s*-polarized obliquely

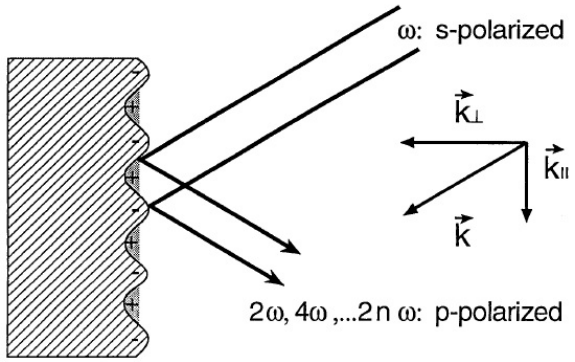

Fig. 1.12: Charge distribution at the plasma-vacuum boundary. Plus and minus represents constant positive background charge due to fixed ions and the negative charge due to back and forth electron motion across the boundary respectively [160].

incident laser, the dipole sheet oscillates at 2ω and it radiates *p*-polarized even harmonics and *s*-polarized odd harmonics. In case of *p*-polarized obliquely incident laser, *p*-polarized even and odd harmonics are generated. For normally incident laser, only odd harmonics are generated [160, 162].

The first experiments on generation of harmonics from solid surfaces were performed by Burnett et al. [164] and Carman et al. [165] with nanosecond CO_2 laser pulses and the generation of harmonics up to 11^{th} and 46^{th} order were observed respectively. With the advent of CPA technique and availability of picosecond and femtosecond lasers, generation of harmonics from solid surfaces was also observed by using lasers of such type. von der Linde and Rzàzewski [166] have observed harmonic generation of a 800 nm (130 fs, 30 mJ) Ti:Sapphire laser up to 18^{th} order reflected from solid surfaces. Kohlweyer et al. [167] have observed the generation of harmonics up to 7^{th} order reflected from solid Al targets irradiated at intensities of 10^{17} W/cm^2. Norreys et al. [168] have detected harmonics spread over a large solid angle up to 75^{th} at wavelengths 14 nm order of a 1053 nm, 2.5 ps Nd:Glass laser. Dromey et al. [169] have reported the generation of harmonics up to 850^{th} order at wavelengths $<$ 4 nm of 1054 nm, 600 fs Vulcan Petawatt laser at intensity $> 10^{20}$ W/cm^2.

1.8 Methodology: Particle-in-Cell (PIC)

Using particle codes to simulate plasma is one of the most direct and powerful approaches particularly to study kinetic and/or nonlinear effects. The key approach deals with dividing the computational space into cells which constitutes a mesh. The mesh is then superimposed on a plasma whose particles can move freely in space from one cell to another in one, two or three dimensions and is hence named as Particle-in-Cell (PIC) as shown in Fig. 1.13. The entire process for Particle-in-Cell

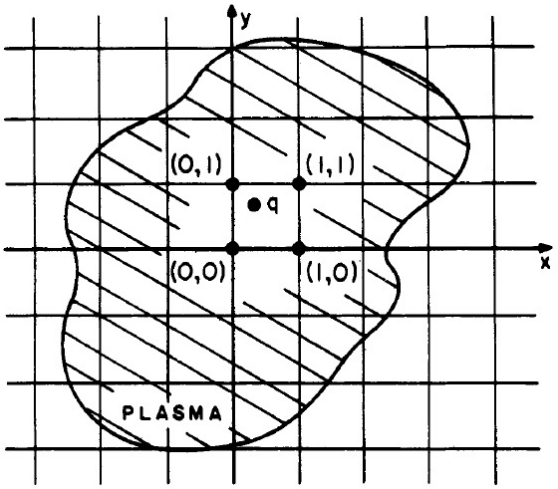

Fig. 1.13: Mathematical grid set into the plasma region in order to measure charge and current densities [170].

(PIC) simulation can be summarized as shown in Fig. 1.14 as follows:

i) The charge and current densities are calculated from the positions and velocities of the particles and are deposited on the spatial grids spatially fine to resolve the collective behaviour using a linear interpolation method.

ii) Using these charge and current densities, the self-consistent electric and magnetic fields are computed using the Maxwell's equations.

iii) These fields are then used to solve the discretized Lorentz force equation to advance the positions and velocities of the charges.

iv) This basic cycle is continued with a time step sufficiently small to resolve the highest frequency in the problem.

The Maxwell's equations are formulated in a finite difference form on the cells. The computational space is divided into cells by the lines which are parallel to the

boundaries and the intersecting points of the lines represents mesh points. The three

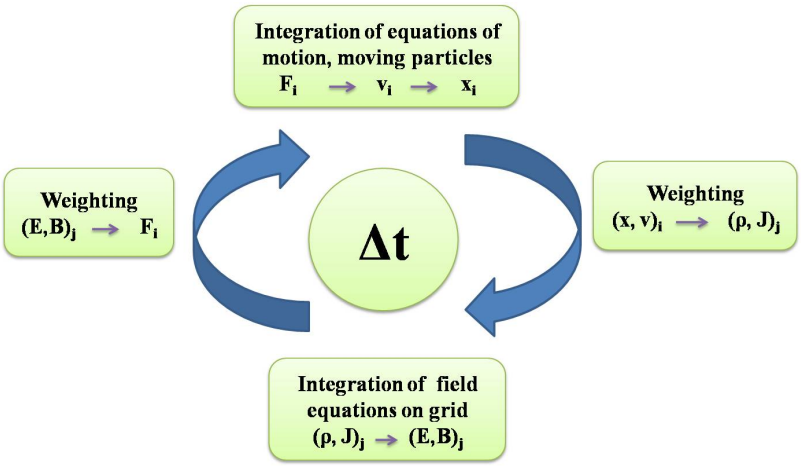

Fig. 1.14: A typical cycle, one time step in a particle in a cell (PIC) simulation program [170].

components of electric and magnetic field vectors along each axes is computed on the mesh points. This way of arranging the electric field, magnetic field and current components is known as the Yee Cell [171] as shown in Fig. 1.15 and is commonly used in the Finite-difference Time-domain (FDTD) method to solve problems related to the propagation, absorption and scattering of electromagnetic waves in dielectrics. The curl of the the fields can be expressed in the space-centered form and by separating the time at which the electric and magnetic fields are computed by half a time increment, the curl equations are time-centered as well.

In the three dimensional case, the indexing of the components in done using the mesh points closest to the origin. For example, the x-component of the electric field positioned at $(i + 1/2, j, k)$ is identified as $E_x(i, j, k)$. Similarly, the x-component of the magnetic field, though positioned at $(i, j+1/2, k+1/2)$, is identified as $B_x(i, j, k)$. During the simulation, the electric fields are known at integer times $(n-1, n, n+1, ...)$, while the magnetic fields and current density are at half integer time $(n - 1/2, n + 1/2, ...)$. Here the time n actually represents a value $n\Delta t$ where Δt is the time increment which represents one complete cycle. The mesh widths along x, y and z directions are represented as Δx, Δy and Δz respectively.

Maxwell's equations are discretized using the FDTD method with reference to the Yee Cell [172–174]. For example, the x-component of the curl of the electric field

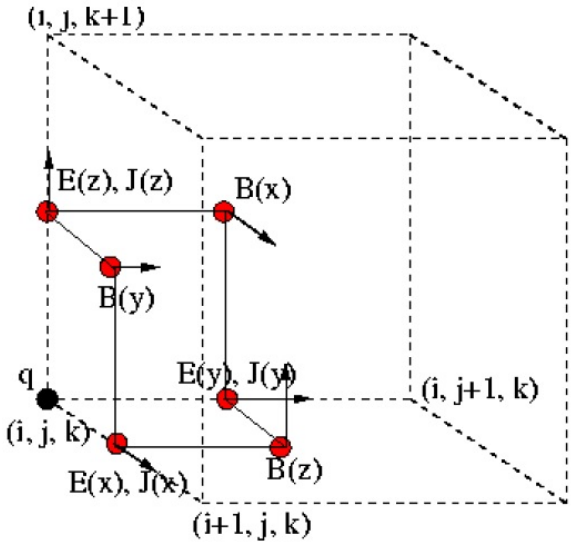

Fig. 1.15: The Yee Cell. The cell vertex labeled (i, j, k) is associated with the components of $\vec{E}$, $\vec{B}$ and $\vec{J}$ displaced by half a cell width at the locations shown above. The charge q is located at the mesh point [171].

at the mesh point (i, j, k) can be written as

$$\frac{E^n_{z(i,j+1,k)} - E^n_{z(i,j,k)}}{\Delta y} - \frac{E^n_{y(i,j,k+1)} - E^n_{y(i,j,k)}}{\Delta z} = -\frac{1}{c}\frac{B^{n+1/2}_{x(i,j,k)} - B^{n-1/2}_{x(i,j,k)}}{\Delta t} \tag{1.42}$$

The above equation is used to advance B_x at mesh point (i, j, k) from step $(n - 1/2)$ to step $(n + 1/2)$ using the values of E_y and E_z at time n at the neighbouring mesh points. Similarly, the x-component of the curl of the magnetic field along the x-direction at the mesh point (i,j,k) can be written as

$$\frac{B^{n+1/2}_{z(i,j,k)} - B^{n+1/2}_{z(i,j-1,k)}}{\Delta y} - \frac{B^{n+1/2}_{y(i,j,k)} - B^{n+1/2}_{y(i,j,k-1)}}{\Delta z} = \frac{4\pi}{c} J^{n+1/2}_{x(i,j,k)} + \frac{E^{n+1}_{x(i,j,k)} - E^n_{x(i,j,k)}}{c\Delta t} \tag{1.43}$$

The above equation is used to advance E_x at mesh point (i, j, k) from step n to step $(n+1)$ using the values of B_y, B_z and J_x at time $(n+1/2)$ at the neighbouring mesh points.

The velocity and position of the particles can be computed by solving the Newton-Lorentz force equation

$$m\frac{d\vec{v}}{dt} = \frac{q}{c}(\vec{E} + \vec{v} \times \vec{B}) \tag{1.44}$$

and

$$\frac{d\vec{x}}{dt} = \vec{v} \tag{1.45}$$

where q and m are the charge and mass of the particle, $\vec{x}$ and $\vec{v}$ are the displacement vector and velocity of the particles respectively. $\vec{E}$ and $\vec{B}$ are the electric and magnetic fields respectively and c is the velocity of light.

The centered-difference form of the Newton-Lorentz force equation can be written as

$$\frac{\vec{v}^{n+1/2} - \vec{v}^{n-1/2}}{\Delta t} = \frac{q}{m}\left(\vec{E} + \frac{\vec{v}^{n+1/2} - \vec{v}^{n-1/2}}{2} \times \vec{B}\right) \tag{1.46}$$

$\vec{E}$ and $\vec{B}$ are now evaluated on the particles instead of mesh points using a linear interpolation method. The computation of particle velocities is carried out in three stages using the Boris method [170]. In this method, the electric and magnetic forces are completely separated taking advantage of the fact that the magnetic field only rotates the direction of the velocity vector without affecting the magnitude whereas the electric field affects both the direction and the magnitude of the velocity vector. In the first stage, the half electric impulse is added to $\vec{v}^{n-1/2}$ to obtain $\vec{v}_-$ such as

$$\vec{v}^{n-1/2} = \vec{v}_- - \frac{q\vec{E}}{m}\frac{\Delta t}{2} \tag{1.47}$$

In the second stage, rotation by $\vec{B}$ is done to obtain $\vec{v}_+$ such as

$$\frac{\vec{v}_+ - \vec{v}_-}{\Delta t} = \frac{q}{2m}(\vec{v}_+ + \vec{v}_-) \times \vec{B} \tag{1.48}$$

In the third stage, the remaining half of the electric impulse is added to $\vec{v}_+$ to obtain $\vec{v}^{n+1/2}$ such as

$$\vec{v}^{n+1/2} = \vec{v}_+ + \frac{q\vec{E}}{m}\frac{\Delta t}{2} \tag{1.49}$$

The angle of rotation θ can be expressed as

$$|tan\frac{\theta}{2}| = \frac{qB}{m}\frac{\Delta t}{2} = \frac{\omega_c \Delta t}{2} \tag{1.50}$$

where $\omega_c = qB/m$ is the cyclotron frequency as shown in Fig. 1.16. The values of $cos\theta$ and $sin\theta$ required for velocity rotation is obtained by using the values of $tan\frac{\theta}{2}$. Taking

$$t = -tan\frac{\theta}{2} \tag{1.51}$$

we have

$$s \equiv -sin\theta = \frac{2t}{1+t^2} \tag{1.52}$$

and

$$c \equiv cos\theta = \frac{1-t^2}{1+t^2} \tag{1.53}$$

According to the Boris method, in order to make a rotation, first $\vec{v}_-$ is incremented

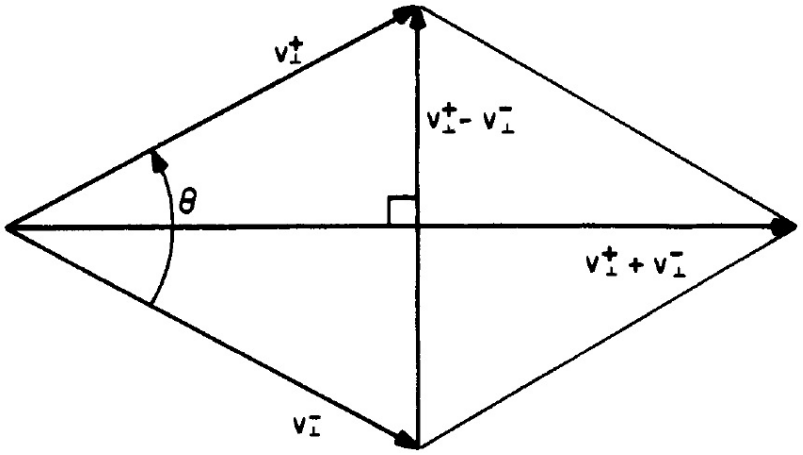

Fig. 1.16: Schematic diagram for the calculation of $tan\frac{\theta}{2}$ [170].

to produce a vector $\vec{v}'$ as shown in Fig. 1.17 such that

$$\vec{v}' = \vec{v}_- + \vec{v}_- \times t \tag{1.54}$$

Thus, $\vec{v}_+$ can be obtained as

$$\vec{v}_+ = \vec{v}_- + \vec{v}' \times s \tag{1.55}$$

The position of the particles can be calculated by the *leap-frog* method as shown in Fig. 1.18 using the relation

$$\frac{d\vec{x}}{dt} = \vec{v} \tag{1.56}$$

which can be written in the time-centered form as

$$\vec{x}^{n+1} = \vec{x}^n + \vec{v}^{n+1/2}\Delta t \tag{1.57}$$

In order to calculate the charge densities at the grid points, a linear interpolation method termed as *weighting* [170] is done among the charged particles and the nearest grid points. In this method, the charged particles are assumed to be of finite

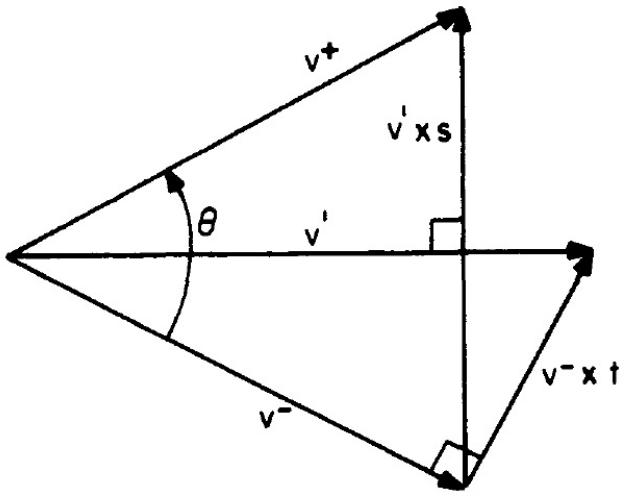

Fig. 1.17: Schematic diagram of the velocity space showing the rotation from $\vec{v}_-$ to $\vec{v}_+$. The velocities shown are the projections of the total velocities onto the plane perpendicular to $\vec{B}$ [170].

sized rigid clouds which may freely pass through each other as shown in Fig. 1.19. Assuming that the charged cloud of charge q_c is of uniform density and Δx wide, the

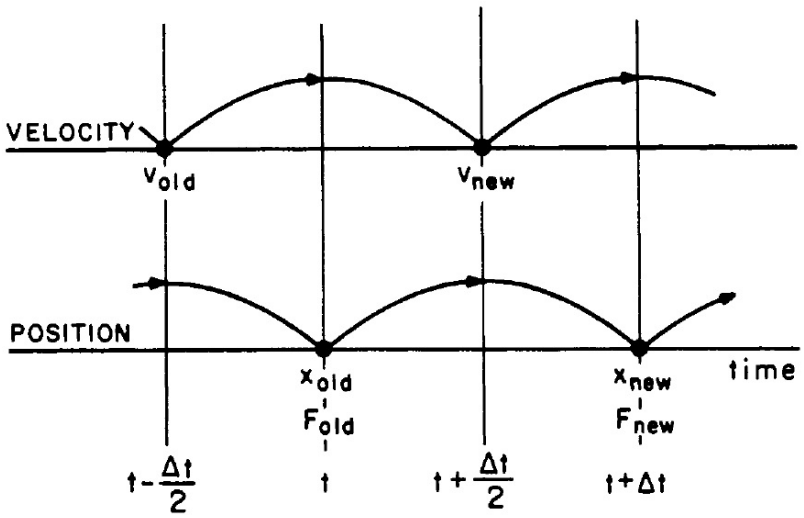

Fig. 1.18: Schematic diagram of leap-frog integration method showing time-centering of force $\vec{F}$ while advancing $\vec{v}$, and of $\vec{v}$ while advancing $\vec{x}$ [170].

fraction of charge assigned to a grid j can be written as

$$q_j = q_c \left[\frac{\Delta x - (x_i - X_j)}{\Delta x} \right] = q_c \left[\frac{X_{j+1} - x_i}{\Delta x} \right] \tag{1.58}$$

and to grid $j+1$ can be written as

$$q_{j+1} = q_c \left[\frac{x_i - X_j}{\Delta x} \right] \tag{1.59}$$

where x_i is the position of charged particle.

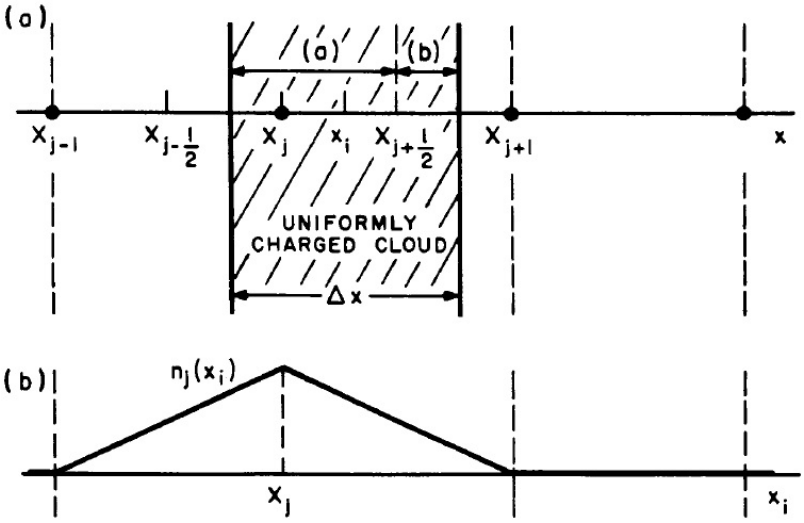

Fig. 1.19: Particle weighting process to calculate charge densities. (a) A part of the charge cloud which is in the j^{th} cell is interpolated at X_j (fraction (a)), and the part of the cloud which is in the $(j+1)^{th}$ cell is interpolated at X_{j+1} (fraction (b)). (b) The grid density $n_j(x_i)$ at point x_i as the particle moves past X_j displaying the effective particle shape $S(x)$ [170].

The field or force weighting on the particle is done in the same way. For example, the electric field $\vec{E}$ interpolated on the particle placed at position x_i can be given as

$$\vec{E}(x_i) = \left[\frac{X_{j+1} - x_i}{\Delta x}\right] \vec{E}_j + \left[\frac{x_i - X_j}{\Delta x}\right] \vec{E}_{j+1} \tag{1.60}$$

The currents at the grids are interpolated from the positions of the particles at time n and $n+1$ and the velocities at time $n+1/2$ and then averaged to obtain $\vec{J}^{n+1/2}$. Thus, the current density $\vec{J}^{n+1/2}$ for a particle at position x_i moving with a velocity $\vec{v}_i^{n+1/2}$ can be given as

$$\vec{J}_j^{n+1/2} = \sum_i q_i \vec{v}_i^{n+1/2} \frac{1}{2} \left[S(X_j - x_i^{n+1}) + S(X_j - x_i^n)\right] \tag{1.61}$$

where $S(x)$ is a spatial interpolation function.

Bibliography

[1] Maine, P., Strickland, D., Bado, P., Pessot, M., and Mourou, G. Generation of ultrahigh peak power pulses by chirped pulse amplification. *IEEE Journal of Quantum Electronics*, 24(2):398–403, 1988.

[2] Mourou, G. The ultrahigh-peak-power laser: present and future. *Applied Physics B*, 65(2):205–211, 1997.

[3] Gibbon, P. *Short Pulse Laser Interactions with Matter: An Introduction*. Imperial College Press, 2005.

[4] Jaroszynski, D., Bingham, R., and Cairns, R. *Laser-Plasma Interactions*. Scottish Graduate Series. CRC Press/Taylor & Francis, 2009.

[5] Tajima, T. and Dawson, J. M. Laser electron accelerator. *Phys. Rev. Lett.*, 43: 267–270, 1979.

[6] Esarey, E., Sprangle, P., Krall, J., and Ting, A. Overview of plasma-based accelerator concepts. *IEEE Transactions on Plasma Science*, 24(2):252–288, 1996.

[7] Solem, J. C., Luk, T. S., Boyer, K., and Rhodes, C. K. Prospects for x-ray amplification with charge-displacement self-channeling. *IEEE Journal of Quantum Electronics*, 25(12):2423–2430, 1989.

[8] Lemoff, B. E., Yin, G. Y., Gordon III, C. L., Barty, C. P. J., and Harris, S. E. Demonstration of a 10-hz femtosecond-pulse-driven xuv laser at 41.8 nm in xe ix. *Phys. Rev. Lett.*, 74:1574–1577, 1995.

[9] Tabak, M., Hammer, J., Glinsky, M. E., Kruer, W. L., Wilks, S. C., Woodworth, J., Campbell, E. M., Perry, M. D., and Mason, R. J. Ignition and high gain with ultrapowerful lasers*. *Physics of Plasmas*, 1(5):1626–1634, 1994.

[10] Regan, S. P., Bradley, D. K., Chirokikh, A. V., Craxton, R. S., Meyerhofer, D. D., Seka, W., Short, R. W., Simon, A., Town, R. P. J., Yaakobi, B., III, J. J. C., and Drake, R. P. Laser-plasma interactions in long-scale-length plasmas

under direct-drive national ignition facility conditions. *Physics of Plasmas*, 6 (5):2072–2080, 1999.

[11] Deutsch, C., Furukawa, H., Mima, K., Murakami, M., and Nishihara, K. Interaction physics of the fast ignitor concept. *Phys. Rev. Lett.*, 77:2483–2486, 1996.

[12] McPherson, A., Gibson, G., Jara, H., Johann, U., Luk, T. S., McIntyre, I. A., Boyer, K., and Rhodes, C. K. Studies of multiphoton production of vacuum-ultraviolet radiation in the rare gases. *J. Opt. Soc. Am. B*, 4(4):595–601, 1987.

[13] Liu, X., Umstadter, D., Esarey, E., and Ting, A. Harmonic generation by an intense laser pulse in neutral and ionized gases. *IEEE Transactions on Plasma Science*, 21(1):90–94, 1993.

[14] Gibbon, P. High-order harmonic generation in plasmas. *IEEE Journal of Quantum Electronics*, 33(11):1915–1924, 1997.

[15] Siminos, E., Sánchez-Arriaga, G., Saxena, V., and Kourakis, I. Modeling relativistic soliton interactions in overdense plasmas: A perturbed nonlinear schrödinger equation framework. *Phys. Rev. E*, 90:063104, 2014.

[16] Borghesi, M., Bulanov, S., Campbell, D. H., Clarke, R. J., Esirkepov, T. Z., Galimberti, M., Gizzi, L. A., MacKinnon, A. J., Naumova, N. M., Pegoraro, F., Ruhl, H., Schiavi, A., and Willi, O. Macroscopic evidence of soliton formation in multiterawatt laser-plasma interaction. *Phys. Rev. Lett.*, 88:135002, 2002.

[17] Bulanov, S. V., Esirkepov, T. Z., Naumova, N. M., Pegoraro, F., and Vshivkov, V. A. Solitonlike electromagnetic waves behind a superintense laser pulse in a plasma. *Phys. Rev. Lett.*, 82:3440–3443, 1999.

[18] Liu, C. and Tripathi, V. *Interaction of Electromagnetic Waves with Electron Beams and Plasmas*. World Scientific, 1994.

[19] Kruer, W. *The physics of laser plasma interactions*. Frontiers in physics. Addison-Wesley, 1988.

[20] Chen, F. F. *Introduction to Plasma Physics and Controlled Fusion*. Springer, 1984.

[21] Gordon, D., Tzeng, K. C., Clayton, C. E., Dangor, A. E., Malka, V., Marsh, K. A., Modena, A., Mori, W. B., Muggli, P., Najmudin, Z., Neely, D., Danson, C., and Joshi, C. Observation of electron energies beyond the linear dephasing limit from a laser-excited relativistic plasma wave. *Phys. Rev. Lett.*, 80:2133–2136, 1998.

[22] Malka, V., Fritzler, S., Lefebvre, E., Aleonard, M.-M., Burgy, F., Chambaret, J.-P., Chemin, J.-F., Krushelnick, K., Malka, G., Mangles, S. P. D., Najmudin, Z., Pittman, M., Rousseau, J.-P., Scheurer, J.-N., Walton, B., and Dangor, A. E. Electron acceleration by a wake field forced by an intense ultrashort laser pulse. *Science*, 298(5598):1596–1600, 2002.

[23] Cid-Vidal, X. and Cid, R. Lhc: the emptiest space in the solar system. *Physics Education*, 46(1):45, 2011.

[24] Gorbunov, L. and Kirsanov, V. Excitation of plasma waves by an electromagnetic wave packet. *Sov. Phys. JETP*, 66(290-294):40, 1987.

[25] Sprangle, P., Joyce, G., Esarey, E., and Ting, A. Laser wakefield acceleration and relativstic optical guiding. *AIP Conference Proceedings*, 175(1):231–239, 1988.

[26] Joshi, C. and Katsouleas, T. Plasma accelerators at the energy frontier and on tabletops. *Physics Today*, 56(6):47–53, 2003.

[27] Hamster, H., Sullivan, A., Gordon, S., White, W., and Falcone, R. W. Subpicosecond, electromagnetic pulses from intense laser-plasma interaction. *Phys. Rev. Lett.*, 71:2725–2728, 1993.

[28] Rosenbluth, M. N. and Liu, C. S. Excitation of plasma waves by two laser beams. *Phys. Rev. Lett.*, 29:701–705, 1972.

[29] Joshi, C., Mori, W., Katsouleas, T., Dawson, J., Kindel, J., and Forslund, D. Ultrahigh gradient particle acceleration by intense laser-driven plasma density waves. *Nature*, 311(5986):525, 1984.

[30] Mourou, G. and Umstadter, D. Development and applications of compact highintensity lasers. *Physics of Fluids B: Plasma Physics*, 4(7):2315–2325, 1992.

[31] Perry, M. D. and Mourou, G. Terawatt to petawatt subpicosecond lasers. *Science*, 264(5161):917–924, 1994.

[32] Joshi, C. The development of laser- and beam-driven plasma accelerators as an experimental field. *Physics of Plasmas*, 14(5):055501, 2007.

[33] Forslund, D. W., Kindel, J. M., Mori, W. B., Joshi, C., and Dawson, J. M. Two-dimensional simulations of single-frequency and beat-wave laser-plasma heating. *Phys. Rev. Lett.*, 54:558–561, 1985.

[34] Clayton, C. E., Joshi, C., Darrow, C., and Umstadter, D. Relativistic plasma-wave excitation by collinear optical mixing. *Phys. Rev. Lett.*, 54:2343–2346, 1985.

[35] Kitagawa, Y., Matsumoto, T., Minamihata, T., Sawai, K., Matsuo, K., Mima, K., Nishihara, K., Azechi, H., Tanaka, K. A., Takabe, H., and Nakai, S. Beat-wave excitation of plasma wave and observation of accelerated electrons. *Phys. Rev. Lett.*, 68:48–51, 1992.

[36] Clayton, C. E., Marsh, K. A., Dyson, A., Everett, M., Lal, A., Leemans, W. P., Williams, R., and Joshi, C. Ultrahigh-gradient acceleration of injected electrons by laser-excited relativistic electron plasma waves. *Phys. Rev. Lett.*, 70:37–40, 1993.

[37] Amiranoff, F., Baton, S., Bernard, D., Cros, B., Descamps, D., Dorchies, F., Jacquet, F., Malka, V., Marquès, J. R., Matthieussent, G., Miné, P., Modena, A., Mora, P., Morillo, J., and Najmudin, Z. Observation of laser wakefield acceleration of electrons. *Phys. Rev. Lett.*, 81:995–998, 1998.

[38] Tochitsky, S. Y., Narang, R., Filip, C. V., Musumeci, P., Clayton, C. E., Yoder, R. B., Marsh, K. A., Rosenzweig, J. B., Pellegrini, C., and Joshi, C. Enhanced acceleration of injected electrons in a laser-beat-wave-induced plasma channel. *Phys. Rev. Lett.*, 92:095004, 2004.

[39] Shvets, G., Fisch, N. J., and Pukhov, A. Excitation of accelerating plasma waves by counter-propagating laser beams. *Physics of Plasmas*, 9(5):2383–2392, 2002.

[40] Joshi, C., Tajima, T., Dawson, J. M., Baldis, H. A., and Ebrahim, N. A. Forward raman instability and electron acceleration. *Phys. Rev. Lett.*, 47:1285–1288, 1981.

[41] Sprangle, P., Esarey, E., Krall, J., and Joyce, G. Propagation and guiding of intense laser pulses in plasmas. *Phys. Rev. Lett.*, 69:2200–2203, 1992.

[42] Nakajima, K., Fisher, D., Kawakubo, T., Nakanishi, H., Ogata, A., Kato, Y., Kitagawa, Y., Kodama, R., Mima, K., Shiraga, H., Suzuki, K., Yamakawa, K., Zhang, T., Sakawa, Y., Shoji, T., Nishida, Y., Yugami, N., Downer, M., and Tajima, T. Observation of ultrahigh gradient electron acceleration by a self-modulated intense short laser pulse. *Phys. Rev. Lett.*, 74:4428–4431, 1995.

[43] Esarey, E., Schroeder, C. B., and Leemans, W. P. Physics of laser-driven plasma-based electron accelerators. *Rev. Mod. Phys.*, 81:1229–1285, 2009.

[44] Krall, J., Ting, A., Esarey, E., and Sprangle, P. Enhanced acceleration in a self-modulated-laser wake-field accelerator. *Phys. Rev. E*, 48:2157–2161, 1993.

[45] Coverdale, C. A., Darrow, C. B., Decker, C. D., Mori, W. B., Tzeng, K.-C., Marsh, K. A., Clayton, C. E., and Joshi, C. Propagation of intense subpicosecond laser pulses through underdense plasmas. *Phys. Rev. Lett.*, 74:4659–4662, 1995.

[46] Modena, A., Najmudin, Z., Dangor, A., Clayton, C., Marsh, K., Joshi, C., Malka, V., Darrow, C., Danson, C., Neely, D., et al. Electron acceleration from the breaking of relativistic plasma waves. *Nature*, 377(6550):606, 1995.

[47] Mangles, S. P., Murphy, C., Najmudin, Z., Thomas, A. G. R., Collier, J., Dangor, A. E., Divall, E., Foster, P., Gallacher, J., Hooker, C., et al. Monoenergetic beams of relativistic electrons from intense laser–plasma interactions. *Nature*, 431(7008):535, 2004.

[48] Geddes, C., Toth, C., Van Tilborg, J., Esarey, E., Schroeder, C., Bruhwiler, D., Nieter, C., Cary, J., and Leemans, W. High-quality electron beams from a laser wakefield accelerator using plasma-channel guiding. *Nature*, 431(7008): 538, 2004.

[49] Faure, J., Rechatin, C., Norlin, A., Lifschitz, A., Glinec, Y., and Malka, V. Controlled injection and acceleration of electrons in plasma wakefields by colliding laser pulses. *Nature*, 444(7120):737, 2006.

[50] Blumenfeld, I., Clayton, C. E., Decker, F.-J., Hogan, M. J., Huang, C., Ischebeck, R., Iverson, R., Joshi, C., Katsouleas, T., Kirby, N., et al. Energy doubling of 42 gev electrons in a metre-scale plasma wakefield accelerator. *Nature*, 445(7129):741, 2007.

[51] Umstadter, D., Chen, S.-Y., Maksimchuk, A., Mourou, G., and Wagner, R. Nonlinear optics in relativistic plasmas and laser wake field acceleration of electrons. *Science*, 273(5274):472–475, 1996.

[52] Malka, V., Fritzler, S., Lefebvre, E., Aleonard, M.-M., Burgy, F., Chambaret, J.-P., Chemin, J.-F., Krushelnick, K., Malka, G., Mangles, S. P. D., Najmudin, Z., Pittman, M., Rousseau, J.-P., Scheurer, J.-N., Walton, B., and Dangor, A. E. Electron acceleration by a wake field forced by an intense ultrashort laser pulse. *Science*, 298(5598):1596–1600, 2002.

[53] Leemans, W. P., Nagler, B., Gonsalves, A. J., Tóth, C., Nakamura, K., Geddes, C. G., Esarey, E., Schroeder, C., and Hooker, S. Gev electron beams from a centimetre-scale accelerator. *Nature physics*, 2(10):696, 2006.

[54] Clayton, C. E., Ralph, J. E., Albert, F., Fonseca, R. A., Glenzer, S. H., Joshi, C., Lu, W., Marsh, K. A., Martins, S. F., Mori, W. B., Pak, A., Tsung, F. S., Pollock, B. B., Ross, J. S., Silva, L. O., and Froula, D. H. Self-guided laser wakefield acceleration beyond 1 gev using ionization-induced injection. *Phys. Rev. Lett.*, 105:105003, 2010.

[55] Wang, X., Zgadzaj, R., Fazel, N., Li, Z., Yi, S., Zhang, X., Henderson, W., Chang, Y.-Y., Korzekwa, R., Tsai, H.-E., et al. Quasi-monoenergetic laser-

plasma acceleration of electrons to 2 gev. *Nature communications*, 4:1988, 2013.

[56] Kim, H. T., Pae, K. H., Cha, H. J., Kim, I. J., Yu, T. J., Sung, J. H., Lee, S. K., Jeong, T. M., and Lee, J. Enhancement of electron energy to the multi-gev regime by a dual-stage laser-wakefield accelerator pumped by petawatt laser pulses. *Phys. Rev. Lett.*, 111:165002, 2013.

[57] Leemans, W. P., Gonsalves, A. J., Mao, H.-S., Nakamura, K., Benedetti, C., Schroeder, C. B., Tóth, C., Daniels, J., Mittelberger, D. E., Bulanov, S. S., Vay, J.-L., Geddes, C. G. R., and Esarey, E. Multi-gev electron beams from capillary-discharge-guided subpetawatt laser pulses in the self-trapping regime. *Phys. Rev. Lett.*, 113:245002, 2014.

[58] Wilks, S. C., Kruer, W. L., Tabak, M., and Langdon, A. B. Absorption of ultra-intense laser pulses. *Phys. Rev. Lett.*, 69:1383–1386, 1992.

[59] Brunel, F. Not-so-resonant, resonant absorption. *Phys. Rev. Lett.*, 59:52–55, 1987.

[60] Kruer, W. L. and Estabrook, K. Jb heating by very intense laser light. *The Physics of Fluids*, 28(1):430–432, 1985.

[61] Yan, X. Q., Lin, C., Sheng, Z. M., Guo, Z. Y., Liu, B. C., Lu, Y. R., Fang, J. X., and Chen, J. E. Generating high-current monoenergetic proton beams by a circularly polarized laser pulse in the phase-stable acceleration regime. *Phys. Rev. Lett.*, 100:135003, 2008.

[62] Macchi, A., Borghesi, M., and Passoni, M. Ion acceleration by superintense laser-plasma interaction. *Rev. Mod. Phys.*, 85:751–793, 2013.

[63] Davies, J. R., Bell, A. R., Haines, M. G., and Guérin, S. M. Short-pulse high-intensity laser-generated fast electron transport into thick solid targets. *Phys. Rev. E*, 56:7193–7203, 1997.

[64] Passoni, M., Tikhonchuk, V. T., Lontano, M., and Bychenkov, V. Y. Charge separation effects in solid targets and ion acceleration with a two-temperature electron distribution. *Phys. Rev. E*, 69:026411, 2004.

[65] Witte, K., Gahn, C., ter Vehn, J. M., Pretzler, G., Pukhov, A., and Tsakiris, G. Physics of ultra-intense laser-plasma interaction. *Plasma Physics and Controlled Fusion*, 41(12B):B221, 1999.

[66] Roth, M., Cowan, T. E., Key, M. H., Hatchett, S. P., Brown, C., Fountain, W., Johnson, J., Pennington, D. M., Snavely, R. A., Wilks, S. C., Yasuike, K., Ruhl, H., Pegoraro, F., Bulanov, S. V., Campbell, E. M., Perry, M. D., and Powell, H. Fast ignition by intense laser-accelerated proton beams. *Phys. Rev. Lett.*, 86:436–439, 2001.

[67] King, N., Ables, E., Adams, K., Alrick, K., Amann, J., Balzar, S., Jr, P. B., Crow, M., Cushing, S., Eddleman, J., Fife, T., Flores, P., Fujino, D., Gallegos, R., Gray, N., Hartouni, E., Hogan, G., Holmes, V., Jaramillo, S., Knudsson, J., London, R., Lopez, R., McDonald, T., McClelland, J., Merrill, F., Morley, K., Morris, C., Naivar, F., Parker, E., Park, H., Pazuchanics, P., Pillai, C., Riedel, C., Sarracino, J., Jr, F. S., Stacy, H., Takala, B., Thompson, R., Tucker, H., Yates, G., Ziock, H.-J., and Zumbro, J. An 800-mev proton radiography facility for dynamic experiments. *Nuclear Instruments and Methods in Physics Research Section A: Accelerators, Spectrometers, Detectors and Associated Equipment*, 424(1):84 – 91, 1999.

[68] Borghesi, M., Schiavi, A., Campbell, D. H., Haines, M. G., Willi, O., Mackinnon, A. J., Patel, P., Galimberti, M., and Gizzi, L. A. Proton imaging detection of transient electromagnetic fields in laser-plasma interactions (invited). *Review of Scientific Instruments*, 74(3):1688–1693, 2003.

[69] Bychenkov, V. Y., Tikhonchuk, V. T., and Tolokonnikov, S. V. Nuclear reactions triggered by laser-accelerated high-energy ions. *Journal of Experimental and Theoretical Physics*, 88(6):1137–1142, 1999.

[70] Khoroshkov, V. S. and Minakova, E. I. Proton beams in radiotherapy. *European Journal of Physics*, 19(6):523, 1998.

[71] Bulanov, S., Esirkepov, T., Khoroshkov, V., Kuznetsov, A., and Pegoraro, F. Oncological hadrontherapy with laser ion accelerators. *Physics Letters A*, 299 (2):240–247, 2002.

[72] Remington, B. A., Drake, R. P., Takabe, H., and Arnett, D. A review of astrophysics experiments on intense lasers. *Physics of Plasmas*, 7(5):1641–1652, 2000.

[73] Gitomer, S. J., Jones, R. D., Begay, F., Ehler, A. W., Kephart, J. F., and Kristal, R. Fast ions and hot electrons in the laserplasma interaction. *The Physics of Fluids*, 29(8):2679–2688, 1986.

[74] Fews, A. P., Norreys, P. A., Beg, F. N., Bell, A. R., Dangor, A. E., Danson, C. N., Lee, P., and Rose, S. J. Plasma ion emission from high intensity picosecond laser pulse interactions with solid targets. *Phys. Rev. Lett.*, 73:1801–1804, 1994.

[75] Krushelnick, K., Clark, E. L., Najmudin, Z., Salvati, M., Santala, M. I. K., Tatarakis, M., Dangor, A. E., Malka, V., Neely, D., Allott, R., and Danson, C. Multi-mev ion production from high-intensity laser interactions with underdense plasmas. *Phys. Rev. Lett.*, 83:737–740, 1999.

[76] Sarkisov, G. S., Bychenkov, V. Y., Novikov, V. N., Tikhonchuk, V. T., Maksimchuk, A., Chen, S.-Y., Wagner, R., Mourou, G., and Umstadter, D. Self-focusing, channel formation, and high-energy ion generation in interaction of an intense short laser pulse with a he jet. *Phys. Rev. E*, 59:7042–7054, 1999.

[77] Ditmire, T., Tisch, J. G., Springate, E., Mason, M., Hay, N., Smith, R., Marangos, J., and Hutchinson, M. High-energy ions produced in explosions of superheated atomic clusters. *Nature*, 386(6620):54, 1997.

[78] Ditmire, T., Zweiback, J., Yanovsky, V., Cowan, T., Hays, G., and Wharton, K. Nuclear fusion from explosions of femtosecond laser-heated deuterium clusters. *Nature*, 398(6727):489, 1999.

[79] Clark, E. L., Krushelnick, K., Davies, J. R., Zepf, M., Tatarakis, M., Beg, F. N., Machacek, A., Norreys, P. A., Santala, M. I. K., Watts, I., and Dangor, A. E. Measurements of energetic proton transport through magnetized plasma from intense laser interactions with solids. *Phys. Rev. Lett.*, 84:670–673, 2000.

[80] Maksimchuk, A., Gu, S., Flippo, K., Umstadter, D., and Bychenkov, V. Y. Forward ion acceleration in thin films driven by a high-intensity laser. *Phys. Rev. Lett.*, 84:4108–4111, 2000.

[81] Snavely, R. A., Key, M. H., Hatchett, S. P., Cowan, T. E., Roth, M., Phillips, T. W., Stoyer, M. A., Henry, E. A., Sangster, T. C., Singh, M. S., Wilks, S. C., MacKinnon, A., Offenberger, A., Pennington, D. M., Yasuike, K., Langdon, A. B., Lasinski, B. F., Johnson, J., Perry, M. D., and Campbell, E. M. Intense high-energy proton beams from petawatt-laser irradiation of solids. *Phys. Rev. Lett.*, 85:2945–2948, 2000.

[82] Wilks, S. C., Langdon, A. B., Cowan, T. E., Roth, M., Singh, M., Hatchett, S., Key, M. H., Pennington, D., MacKinnon, A., and Snavely, R. A. Energetic proton generation in ultra-intense lasersolid interactions. *Physics of Plasmas*, 8(2):542–549, 2001.

[83] Hegelich, M., Karsch, S., Pretzler, G., Habs, D., Witte, K., Guenther, W., Allen, M., Blazevic, A., Fuchs, J., Gauthier, J. C., Geissel, M., Audebert, P., Cowan, T., and Roth, M. Mev ion jets from short-pulse-laser interaction with thin foils. *Phys. Rev. Lett.*, 89:085002, 2002.

[84] Mackinnon, A. J., Borghesi, M., Hatchett, S., Key, M. H., Patel, P. K., Campbell, H., Schiavi, A., Snavely, R., Wilks, S. C., and Willi, O. Effect of plasma scale length on multi-mev proton production by intense laser pulses. *Phys. Rev. Lett.*, 86:1769–1772, 2001.

[85] Allen, M., Patel, P. K., Mackinnon, A., Price, D., Wilks, S., and Morse, E. Direct experimental evidence of back-surface ion acceleration from laser-irradiated gold foils. *Phys. Rev. Lett.*, 93:265004, 2004.

[86] Cowan, T. E., Fuchs, J., Ruhl, H., Kemp, A., Audebert, P., Roth, M., Stephens, R., Barton, I., Blazevic, A., Brambrink, E., Cobble, J., Fernández, J., Gauthier, J.-C., Geissel, M., Hegelich, M., Kaae, J., Karsch, S., Le Sage, G. P., Letzring, S., Manclossi, M., Meyroneinc, S., Newkirk, A., Pépin, H., and Renard-LeGalloudec, N. Ultralow emittance, multi-mev proton beams from a laser virtual-cathode plasma accelerator. *Phys. Rev. Lett.*, 92:204801, 2004.

[87] Fuchs, J., Antici, P., dHumières, E., Lefebvre, E., Borghesi, M., Brambrink, E., Cecchetti, C., Kaluza, M., Malka, V., Manclossi, M., et al. Laser-driven proton scaling laws and new paths towards energy increase. *Nature physics*, 2 (1):48, 2006.

[88] Borghesi, M., Fuchs, J., Bulanov, S. V., MacKinnon, A. J., Patel, P. K., and Roth, M. Fast ion generation by high-intensity laser irradiation of solid targets and applications. *Fusion Science and Technology*, 49(3):412–439, 2006.

[89] Zeil, K., Kraft, S. D., Bock, S., Bussmann, M., Cowan, T. E., Kluge, T., Metzkes, J., Richter, T., Sauerbrey, R., and Schramm, U. The scaling of proton energies in ultrashort pulse laser plasma acceleration. *New Journal of Physics*, 12(4):045015, 2010.

[90] Fuchs, J., Cowan, T. E., Audebert, P., Ruhl, H., Gremillet, L., Kemp, A., Allen, M., Blazevic, A., Gauthier, J.-C., Geissel, M., Hegelich, M., Karsch, S., Parks, P., Roth, M., Sentoku, Y., Stephens, R., and Campbell, E. M. Spatial uniformity of laser-accelerated ultrahigh-current mev electron propagation in metals and insulators. *Phys. Rev. Lett.*, 91:255002, 2003.

[91] Roth, M., Blazevic, A., Geissel, M., Schlegel, T., Cowan, T. E., Allen, M., Gauthier, J.-C., Audebert, P., Fuchs, J., Meyer-ter Vehn, J., Hegelich, M., Karsch, S., and Pukhov, A. Energetic ions generated by laser pulses: A detailed study on target properties. *Phys. Rev. ST Accel. Beams*, 5:061301, 2002.

[92] Kaluza, M., Schreiber, J., Santala, M. I. K., Tsakiris, G. D., Eidmann, K., Meyer-ter Vehn, J., and Witte, K. J. Influence of the laser prepulse on proton acceleration in thin-foil experiments. *Phys. Rev. Lett.*, 93:045003, 2004.

[93] Neely, D., Foster, P., Robinson, A., Lindau, F., Lundh, O., Persson, A., Wahlstrm, C.-G., and McKenna, P. Enhanced proton beams from ultrathin targets driven by high contrast laser pulses. *Applied Physics Letters*, 89(2): 021502, 2006.

[94] Psikal, J., Tikhonchuk, V. T., Limpouch, J., Andreev, A. A., and Brantov, A. V. Ion acceleration by femtosecond laser pulses in small multispecies targets. *Physics of Plasmas*, 15(5):053102, 2008.

[95] Buffechoux, S., Psikal, J., Nakatsutsumi, M., Romagnani, L., Andreev, A., Zeil, K., Amin, M., Antici, P., Burris-Mog, T., Compant-La-Fontaine, A., d'Humières, E., Fourmaux, S., Gaillard, S., Gobet, F., Hannachi, F., Kraft, S., Mancic, A., Plaisir, C., Sarri, G., Tarisien, M., Toncian, T., Schramm, U., Tampo, M., Audebert, P., Willi, O., Cowan, T. E., Pépin, H., Tikhonchuk, V., Borghesi, M., and Fuchs, J. Hot electrons transverse refluxing in ultraintense laser-solid interactions. *Phys. Rev. Lett.*, 105:015005, 2010.

[96] Gaillard, S. A., Kluge, T., Flippo, K. A., Bussmann, M., Gall, B., Lockard, T., Geissel, M., Offermann, D. T., Schollmeier, M., Sentoku, Y., and Cowan, T. E. Increased laser-accelerated proton energies via direct laser-light-pressure acceleration of electrons in microcone targets. *Physics of Plasmas*, 18(5):056710, 2011.

[97] Flippo, K. A., dHumires, E., Gaillard, S. A., Rassuchine, J., Gautier, D. C., Schollmeier, M., Nrnberg, F., Kline, J. L., Adams, J., Albright, B., Bakeman, M., Harres, K., Johnson, R. P., Korgan, G., Letzring, S., Malekos, S., Renard-LeGalloudec, N., Sentoku, Y., Shimada, T., Roth, M., Cowan, T. E., Fernndez, J. C., and Hegelich, B. M. Increased efficiency of short-pulse laser-generated proton beams from novel flat-top cone targets. *Physics of Plasmas*, 15(5): 056709, 2008.

[98] Esirkepov, T., Borghesi, M., Bulanov, S. V., Mourou, G., and Tajima, T. Highly efficient relativistic-ion generation in the laser-piston regime. *Phys. Rev. Lett.*, 92:175003, 2004.

[99] Henig, A., Steinke, S., Schnürer, M., Sokollik, T., Hörlein, R., Kiefer, D., Jung, D., Schreiber, J., Hegelich, B. M., Yan, X. Q., Meyer-ter Vehn, J., Tajima, T., Nickles, P. V., Sandner, W., and Habs, D. Radiation-pressure acceleration of ion beams driven by circularly polarized laser pulses. *Phys. Rev. Lett.*, 103: 245003, 2009.

[100] Macchi, A., Cattani, F., Liseykina, T. V., and Cornolti, F. Laser acceleration of ion bunches at the front surface of overdense plasmas. *Phys. Rev. Lett.*, 94: 165003, 2005.

[101] Jackson, J. *Classical electrodynamics*. Wiley, 3 edition, 1975.

[102] Schlegel, T., Naumova, N., Tikhonchuk, V. T., Labaune, C., Sokolov, I. V., and Mourou, G. Relativistic laser piston model: Ponderomotive ion acceleration in dense plasmas using ultraintense laser pulses. *Physics of Plasmas*, 16(8): 083103, 2009.

[103] Naumova, N., Schlegel, T., Tikhonchuk, V. T., Labaune, C., Sokolov, I. V., and Mourou, G. Hole boring in a dt pellet and fast-ion ignition with ultraintense laser pulses. *Phys. Rev. Lett.*, 102:025002, 2009.

[104] Robinson, A. P. L., Gibbon, P., Zepf, M., Kar, S., Evans, R. G., and Bellei, C. Relativistically correct hole-boring and ion acceleration by circularly polarized laser pulses. *Plasma Physics and Controlled Fusion*, 51(2):024004, 2009.

[105] Esirkepov, T., Borghesi, M., Bulanov, S. V., Mourou, G., and Tajima, T. Highly efficient relativistic-ion generation in the laser-piston regime. *Phys. Rev. Lett.*, 92:175003, 2004.

[106] Qiao, B., Zepf, M., Borghesi, M., and Geissler, M. Stable gev ion-beam acceleration from thin foils by circularly polarized laser pulses. *Phys. Rev. Lett.*, 102:145002, 2009.

[107] Denavit, J. Absorption of high-intensity subpicosecond lasers on solid density targets. *Phys. Rev. Lett.*, 69:3052–3055, 1992.

[108] Silva, L. O., Marti, M., Davies, J. R., Fonseca, R. A., Ren, C., Tsung, F. S., and Mori, W. B. Proton shock acceleration in laser-plasma interactions. *Phys. Rev. Lett.*, 92:015002, 2004.

[109] Palmer, C. A. J., Dover, N. P., Pogorelsky, I., Babzien, M., Dudnikova, G. I., Ispiriyan, M., Polyanskiy, M. N., Schreiber, J., Shkolnikov, P., Yakimenko, V., and Najmudin, Z. Monoenergetic proton beams accelerated by a radiation pressure driven shock. *Phys. Rev. Lett.*, 106:014801, 2011.

[110] Badziak, J., Gowacz, S., Jaboski, S., Parys, P., Woowski, J., and Hora, H. Production of ultrahigh-current-density ion beams by short-pulse skin-layer laserplasma interaction. *Applied Physics Letters*, 85(15):3041–3043, 2004.

[111] Akli, K. U., Hansen, S. B., Kemp, A. J., Freeman, R. R., Beg, F. N., Clark, D. C., Chen, S. D., Hey, D., Hatchett, S. P., Highbarger, K., Giraldez, E., Green, J. S., Gregori, G., Lancaster, K. L., Ma, T., MacKinnon, A. J., Norreys, P., Patel, N., Pasley, J., Shearer, C., Stephens, R. B., Stoeckl, C., Storm, M., Theobald, W., Van Woerkom, L. D., Weber, R., and Key, M. H. Laser heating of solid matter by light-pressure-driven shocks at ultrarelativistic intensities. *Phys. Rev. Lett.*, 100:165002, 2008.

[112] Henig, A., Kiefer, D., Geissler, M., Rykovanov, S. G., Ramis, R., Hörlein, R., Osterhoff, J., Major, Z., Veisz, L., Karsch, S., Krausz, F., Habs, D., and Schreiber, J. Laser-driven shock acceleration of ion beams from spherical mass-limited targets. *Phys. Rev. Lett.*, 102:095002, 2009.

[113] Esirkepov, T., Borghesi, M., Bulanov, S. V., Mourou, G., and Tajima, T. Highly efficient relativistic-ion generation in the laser-piston regime. *Phys. Rev. Lett.*, 92:175003, 2004.

[114] Pegoraro, F. and Bulanov, S. V. Photon bubbles and ion acceleration in a plasma dominated by the radiation pressure of an electromagnetic pulse. *Phys. Rev. Lett.*, 99:065002, 2007.

[115] Liseykina, T. V., Borghesi, M., Macchi, A., and Tuveri, S. Radiation pressure acceleration by ultraintense laser pulses. *Plasma Physics and Controlled Fusion*, 50(12):124033, 2008.

[116] Robinson, A. P. L., Zepf, M., Kar, S., Evans, R. G., and Bellei, C. Radiation pressure acceleration of thin foils with circularly polarized laser pulses. *New Journal of Physics*, 10(1):013021, 2008.

[117] Kar, S., Kakolee, K. F., Qiao, B., Macchi, A., Cerchez, M., Doria, D., Geissler, M., McKenna, P., Neely, D., Osterholz, J., Prasad, R., Quinn, K., Ramakrishna, B., Sarri, G., Willi, O., Yuan, X. Y., Zepf, M., and Borghesi, M. Ion acceleration in multispecies targets driven by intense laser radiation pressure. *Phys. Rev. Lett.*, 109:185006, 2012.

[118] Henig, A., Steinke, S., Schnürer, M., Sokollik, T., Hörlein, R., Kiefer, D., Jung, D., Schreiber, J., Hegelich, B. M., Yan, X. Q., Meyer-ter Vehn, J., Tajima, T.,

Nickles, P. V., Sandner, W., and Habs, D. Radiation-pressure acceleration of ion beams driven by circularly polarized laser pulses. *Phys. Rev. Lett.*, 103: 245003, 2009.

[119] Haberberger, D., Tochitsky, S., Fiuza, F., Gong, C., Fonseca, R. A., Silva, L. O., Mori, W. B., and Joshi, C. Collisionless shocks in laser-produced plasma generate monoenergetic high-energy proton beams. *Nature Physics*, 8(1):95, 2012.

[120] Kim, I. J., Pae, K. H., Choi, I. W., Lee, C.-L., Kim, H. T., Singhal, H., Sung, J. H., Lee, S. K., Lee, H. W., Nickles, P. V., Jeong, T. M., Kim, C. M., and Nam, C. H. Radiation pressure acceleration of protons to 93mev with circularly polarized petawatt laser pulses. *Physics of Plasmas*, 23(7):070701, 2016.

[121] Yin, L., Albright, B. J., Hegelich, B. M., and Fernandez, J. C. Gev laser ion acceleration from ultrathin targets: The laser break-out afterburner. *Laser and Particle Beams*, 24(2):291298, 2006.

[122] Yin, L., Albright, B. J., Hegelich, B. M., Bowers, K. J., Flippo, K. A., Kwan, T. J. T., and Fernndez, J. C. Monoenergetic and gev ion acceleration from the laser breakout afterburner using ultrathin targets. *Physics of Plasmas*, 14(5): 056706, 2007.

[123] Bulanov, S. V. and Esirkepov, T. Z. Comment on "collimated multi-mev ion beams from high-intensity laser interactions with underdense plasma". *Phys. Rev. Lett.*, 98:049503, 2007.

[124] Fukuda, Y., Faenov, A. Y., Tampo, M., Pikuz, T. A., Nakamura, T., Kando, M., Hayashi, Y., Yogo, A., Sakaki, H., Kameshima, T., Pirozhkov, A. S., Ogura, K., Mori, M., Esirkepov, T. Z., Koga, J., Boldarev, A. S., Gasilov, V. A., Magunov, A. I., Yamauchi, T., Kodama, R., Bolton, P. R., Kato, Y., Tajima, T., Daido, H., and Bulanov, S. V. Energy increase in multi-mev ion acceleration in the interaction of a short pulse laser with a cluster-gas target. *Phys. Rev. Lett.*, 103:165002, 2009.

[125] Nakamura, T., Bulanov, S. V., Esirkepov, T. Z., and Kando, M. High-energy

ions from near-critical density plasmas via magnetic vortex acceleration. *Phys. Rev. Lett.*, 105:135002, 2010.

[126] Bulanov, S. S., Bychenkov, V. Y., Chvykov, V., Kalinchenko, G., Litzenberg, D. W., Matsuoka, T., Thomas, A. G. R., Willingale, L., Yanovsky, V., Krushelnick, K., and Maksimchuk, A. Generation of gev protons from 1 pw laser interaction with near critical density targets. *Physics of Plasmas*, 17(4):043105, 2010.

[127] Willingale, L., Mangles, S. P. D., Nilson, P. M., Clarke, R. J., Dangor, A. E., Kaluza, M. C., Karsch, S., Lancaster, K. L., Mori, W. B., Najmudin, Z., Schreiber, J., Thomas, A. G. R., Wei, M. S., and Krushelnick, K. Willingale et al. reply:. *Phys. Rev. Lett.*, 98:049504, 2007.

[128] Wilks, S. C., Kruer, W. L., Tabak, M., and Langdon, A. B. Absorption of ultra-intense laser pulses. *Phys. Rev. Lett.*, 69:1383–1386, 1992.

[129] Sandhu, A. S., Dharmadhikari, A. K., Rajeev, P. P., Kumar, G. R., Sengupta, S., Das, A., and Kaw, P. K. Laser-generated ultrashort multimegagauss magnetic pulses in plasmas. *Phys. Rev. Lett.*, 89:225002, 2002.

[130] Mondal, S., Narayanan, V., Ding, W. J., Lad, A. D., Hao, B., Ahmad, S., Wang, W. M., Sheng, Z. M., Sengupta, S., Kaw, P., Das, A., and Kumar, G. R. Direct observation of turbulent magnetic fields in hot, dense laser produced plasmas. *Proceedings of the National Academy of Sciences*, 109(21):8011–8015, 2012.

[131] Tatarakis, M., Watts, I., Beg, F., Clark, E., Dangor, A., Gopal, A., Haines, M., Norreys, P., Wagner, U., Wei, M.-S., et al. Laser technology: Measuring huge magnetic fields. *Nature*, 415(6869):280, 2002.

[132] Tabak, M., Hammer, J., Glinsky, M. E., Kruer, W. L., Wilks, S. C., Woodworth, J., Campbell, E. M., Perry, M. D., and Mason, R. J. Ignition and high gain with ultrapowerful lasers*. *Physics of Plasmas*, 1(5):1626–1634, 1994.

[133] Murnane, M. M., Kapteyn, H. C., Rosen, M. D., and Falcone, R. W. Ultrafast x-ray pulses from laser-produced plasmas. *Science*, 251(4993):531–536, 1991.

[134] Belyaev, V. S., Krainov, V. P., Lisitsa, V. S., and Matafonov, A. P. Generation of fast charged particles and superstrong magnetic fields in the interaction of ultrashort high-intensity laser pulses with solid targets. *Physics-Uspekhi*, 51 (8):793, 2008.

[135] Weibel, E. S. Spontaneously growing transverse waves in a plasma due to an anisotropic velocity distribution. *Phys. Rev. Lett.*, 2:83–84, 1959.

[136] Fried, B. D. Mechanism for instability of transverse plasma waves. *The Physics of Fluids*, 2(3):337–337, 1959.

[137] Schlüter, A. and Biermann, L. Interstellare magnetfelder. *Zeitschrift für Naturforschung A*, 5(5):237–251, 1950.

[138] Stamper, J. A., Papadopoulos, K., Sudan, R. N., Dean, S. O., McLean, E. A., and Dawson, J. M. Spontaneous magnetic fields in laser-produced plasmas. *Phys. Rev. Lett.*, 26:1012–1015, 1971.

[139] Gradov, O. and Stenflo, L. Magnetic-field generation by a finite-radius electromagnetic beam. *Physics Letters A*, 95(5):233 – 234, 1983.

[140] Sudan, R. N. Mechanism for the generation of 10^9 g magnetic fields in the interaction of ultraintense short laser pulse with an overdense plasma target. *Phys. Rev. Lett.*, 70:3075–3078, 1993.

[141] Krausz, F. and Ivanov, M. Attosecond physics. *Rev. Mod. Phys.*, 81:163–234, 2009.

[142] Theobald, W., Häßner, R., Wülker, C., and Sauerbrey, R. Temporally resolved measurement of electron densities ($> 10^{23}$ cm^{-3}) with high harmonics. *Phys. Rev. Lett.*, 77:298–301, 1996.

[143] Merdji, H., Salieres, P., Le Deroff, L., Hergott, J.-F., Carre, B., Joyeux, D., Descamps, D., Norin, J., Lynga, C., L'huillier, A., Wahlstrom, C.-G., Bellini, M., and Huller, S. Coherence properties of high-order harmonics: Application to high-density laserplasma diagnostic. *Laser and Particle Beams*, 18(3): 495502, 2000.

[144] Dobosz, S., Doumy, G., Stabile, H., D'Oliveira, P., Monot, P., Réau, F., Hüller, S., and Martin, P. Probing hot and dense laser-induced plasmas with ultrafast xuv pulses. *Phys. Rev. Lett.*, 95:025001, 2005.

[145] Ramakrishna, S. and Seideman, T. High-order harmonic generation as a probe of rotational dynamics. *Phys. Rev. A*, 77:053411, 2008.

[146] Kanai, T., Takahashi, E. J., Nabekawa, Y., and Midorikawa, K. Observing molecular structures by using high-order harmonic generation in mixed gases. *Phys. Rev. A*, 77:041402, 2008.

[147] Schnürer, M., Cheng, Z., Hentschel, M., Tempea, G., Kálmán, P., Brabec, T., and Krausz, F. Absorption-limited generation of coherent ultrashort soft-x-ray pulses. *Phys. Rev. Lett.*, 83:722–725, 1999.

[148] Sekikawa, T., Kosuge, A., Kanai, T., and Watanabe, S. Nonlinear optics in the extreme ultraviolet. *Nature*, 432(7017):605, 2004.

[149] Tzallas, P., Witte, K., Tsakiris, G., Papadogiannis, N., and Charalambidis, D. Extending optical fs metrology to xuv attosecond pulses. *Applied Physics A*, 79(7):1673–1677, 2004.

[150] Corkum, P. B. Plasma perspective on strong field multiphoton ionization. *Phys. Rev. Lett.*, 71:1994–1997, 1993.

[151] Macklin, J. J., Kmetec, J. D., and Gordon, C. L. High-order harmonic generation using intense femtosecond pulses. *Phys. Rev. Lett.*, 70:766–769, 1993.

[152] Keldysh, L. V. Ionization in the field of a strong electromagnetic wave. *Sov. Phys. JETP*, 20(5):1307–1314, 1965.

[153] Brabec, T. and Krausz, F. Intense few-cycle laser fields: Frontiers of nonlinear optics. *Rev. Mod. Phys.*, 72:545–591, 2000.

[154] McPherson, A., Gibson, G., Jara, H., Johann, U., Luk, T. S., McIntyre, I. A., Boyer, K., and Rhodes, C. K. Studies of multiphoton production of vacuum-ultraviolet radiation in the rare gases. *J. Opt. Soc. Am. B*, 4(4):595–601, 1987.

[155] Crane, J. K., Perry, M. D., Herman, S., and Falcone, R. W. High-field harmonic generation in helium. *Opt. Lett.*, 17(18):1256–1258, 1992.

[156] L'Huillier, A. and Balcou, P. High-order harmonic generation in rare gases with a 1-ps 1053-nm laser. *Phys. Rev. Lett.*, 70:774–777, 1993.

[157] Macklin, J. J., Kmetec, J. D., and Gordon, C. L. High-order harmonic generation using intense femtosecond pulses. *Phys. Rev. Lett.*, 70:766–769, 1993.

[158] Chang, Z., Rundquist, A., Wang, H., Murnane, M. M., and Kapteyn, H. C. Generation of coherent soft x rays at 2.7 nm using high harmonics. *Phys. Rev. Lett.*, 79:2967–2970, 1997.

[159] Spielmann, C., Burnett, N. H., Sartania, S., Koppitsch, R., Schnürer, M., Kan, C., Lenzner, M., Wobrauschek, P., and Krausz, F. Generation of coherent x-rays in the water window using 5-femtosecond laser pulses. *Science*, 278(5338): 661–664, 1997.

[160] von der Linde, D. and Rzàzewski, K. High-order optical harmonic generation from solid surfaces. *Applied Physics B*, 63(5):499–506, 1996.

[161] von der Linde, D. Generation of high order optical harmonics from solid surfaces. *Applied Physics B*, 68(3):315–319, 1999.

[162] Lichters, R., MeyerterVehn, J., and Pukhov, A. Shortpulse laser harmonics from oscillating plasma surfaces driven at relativistic intensity. *Physics of Plasmas*, 3(9):3425–3437, 1996.

[163] Umstadter, D. Relativistic laserplasma interactions. *Journal of Physics D: Applied Physics*, 36(8):R151, 2003.

[164] Burnett, N. H., Baldis, H. A., Richardson, M. C., and Enright, G. D. Harmonic generation in co2 laser target interaction. *Applied Physics Letters*, 31(3):172–174, 1977.

[165] Carman, R. L., Forslund, D. W., and Kindel, J. M. Visible harmonic emission as a way of measuring profile steepening. *Phys. Rev. Lett.*, 46:29–32, 1981.

[166] von der Linde, D. and Rzàzewski, K. High-order optical harmonic generation from solid surfaces. *Applied Physics B*, 63(5):499–506, 1996.

[167] Kohlweyer, S., Tsakiris, G., Wahlstrm, C.-G., Tillman, C., and Mercer, I. Harmonic generation from solid-vacuum interface irradiated at high laser intensities. *Optics Communications*, 117(5):431 – 438, 1995.

[168] Norreys, P. A., Zepf, M., Moustaizis, S., Fews, A. P., Zhang, J., Lee, P., Bakarezos, M., Danson, C. N., Dyson, A., Gibbon, P., Loukakos, P., Neely, D., Walsh, F. N., Wark, J. S., and Dangor, A. E. Efficient extreme uv harmonics generated from picosecond laser pulse interactions with solid targets. *Phys. Rev. Lett.*, 76:1832–1835, 1996.

[169] Dromey, B., Zepf, M., Gopal, A., Lancaster, K., Wei, M., Krushelnick, K., Tatarakis, M., Vakakis, N., Moustaizis, S., Kodama, R., et al. High harmonic generation in the relativistic limit. *Nature physics*, 2(7):456, 2006.

[170] Birdsall, C. and Langdon, A. *Plasma Physics via Computer Simulation*. Series in Plasma Physics and Fluid Dynamics. Taylor & Francis, 2004.

[171] Yee, K. Numerical solution of initial boundary value problems involving maxwell's equations in isotropic media. *IEEE Transactions on Antennas and Propagation*, 14(3):302–307, 1966.

[172] Sadiku, M. *Numerical Techniques in Electromagnetics, Second Edition*. CRC Press, 2000.

[173] Sullivan, D. *Electromagnetic Simulation Using the FDTD Method*. IEEE Press Series on RF and Microwave Technology. Wiley, 2000.

[174] Sui, W. *Time-Domain Computer Analysis of Nonlinear Hybrid Systems*. CRC Press, 2001.